1976

Turbulent flux estimates from shipboard mean wind and temperature profiles and dissipation rates

Atkinson, Harvey Eugene

Monterey, California. Naval Postgraduate School

TURBULENT FLUX ESTIMATES FROM SHIPBOARD MEAN WIND AND TEMPERATURE PROFILES AND DISSIPATION RATES

Harvey Eugene Atkinson

NAVAL POSTGRADUATE SCHOOL
Monterey, California

THESIS

TURBULENT FLUX ESTIMATES
FROM SHIPBOARD MEAN WIND
AND
TEMPERATURE PROFILES AND DISSIPATION RATES

by

Harvey Eugene Atkinson III

March 1976

Thesis Advisor: Kenneth L. Davidson

Approved for public release; distribution unlimited.

SECURITY CLASSIFICATION OF THIS PAGE (When Data Entered)

REPORT DOCUMENTATION PAGE		READ INSTRUCTIONS BEFORE COMPLETING FORM
1. REPORT NUMBER	2. GOVT ACCESSION NO.	3. RECIPIENT'S CATALOG NUMBER
4. TITLE (and Subtitle) TURBULENT FLUX ESTIMATES FROM SHIPBOARD MEAN WIND AND TEMPERATURE PROFILES AND DISSIPATION RATES		5. TYPE OF REPORT & PERIOD COVERED Master's Thesis, March, 1976 6. PERFORMING ORG. REPORT NUMBER
7. AUTHOR(s) Harvey Eugene Atkinson III		8. CONTRACT OR GRANT NUMBER(s)
9. PERFORMING ORGANIZATION NAME AND ADDRESS Naval Postgraduate School Monterey, California 93940		10. PROGRAM ELEMENT, PROJECT, TASK AREA & WORK UNIT NUMBERS
11. CONTROLLING OFFICE NAME AND ADDRESS Naval Postgraduate School Monterey, California 93940		12. REPORT DATE March 1976 13. NUMBER OF PAGES
14. MONITORING AGENCY NAME & ADDRESS(if different from Controlling Office)		15. SECURITY CLASS. (of this report) Unclassified 15a. DECLASSIFICATION/DOWNGRADING SCHEDULE

16. DISTRIBUTION STATEMENT (of this Report)

Approved for public release; distribution unlimited.

17. DISTRIBUTION STATEMENT (of the abstract entered in Block 20, if different from Report)

18. SUPPLEMENTARY NOTES

19. KEY WORDS (Continue on reverse side if necessary and identify by block number)

20. ABSTRACT (Continue on reverse side if necessary and identify by block number)

Height profiles of mean wind speed and wind velocity fluctuation spectra are derived from observations made aboard the R/V Acania while anchored in Monterey Bay. The profiles and spectra in conjunction with related temperature fluctuation data obtained in a parallel study are used to calculate the atmospheric boundary layer turbulence parameters: friction velocity U_*, drag coefficient C_D, vertical heat flux ($\overline{w'T'}$) and z/L. A general disagreement of the results of this study with each other and with previously published

DD FORM 1 JAN 73 1473 EDITION OF 1 NOV 65 IS OBSOLETE
S/N 0102-014-6601 |
(Page 1)

SECURITY CLASSIFICATION OF THIS PAGE (When Data Entered)

results is inconclusive due to small size of the data base. The best agreement with results of other studies was with the calculation of the drag coefficient using velocity fluctuation data.

TURBULENT FLUX ESTIMATES FROM SHIPBOARD MEAN WIND

AND

TEMPERATURE PROFILES AND DISSIPATION RATES

by

Harvey Eugene Atkinson III
Lieutenant, United States Navy
B.S., Virginia Polytechnic Institute, 1965

Submitted in partial fulfillment of the
requirements for the degree of

MASTER OF SCIENCE IN METEOROLOGY

from the

NAVAL POSTGRADUATE SCHOOL
March 1976

ABSTRACT

Height profiles of mean wind speed and wind velocity fluctuation spectra are derived from observations made aboard the R/V Acania while anchored in Monterey Bay. The profiles and spectra in conjunction with related temperature fluctuation data obtained in a parallel study are used to calculate the atmospheric boundary layer turbulence parameters: friction velocity, U_*, drag coefficient, C_D, vertical heat flux ($\overline{w'T'}$) and z/L. A general disagreement of the results of this study with each other and with previously published results is inconclusive due to small size of the data base. The best agreement with results of other studies was with the calculation of the drag coefficient using velocity fluctuation data.

TABLE OF CONTENTS

LIST OF TABLES

LIST OF FIGURES

ACKNOWLEDGEMENTS

I feel that Dr. Kenneth L. Davidson deserves very special thanks for many long hours of patient guidance and support. Dr. Thomas Houlihan was a great deal of help in furthering my understanding of the data processing equipment used in this study. My thanks also to Mr. Charles Leonard and Mr. Steve Rinard for their help in processing the raw data used herein. I thank also Lt. Michelle Hughes for providing some of the data necessary for the completion of this study. And to Lcdr. Benny Hassel and Mr. Michael McDermet my thanks for their assistance in much of the drafting done for this thesis. I thank Gail Roy, my typist, for the hours she spent working with me in order to get things just the way I wanted them.

Finally, to my wife, Barbara, goes my deepest gratitude. Her endless patience and understanding together with countless hours of typing roughs made my work much much easier.

I. INTRODUCTION

In recent years the turbulent structure of the atmospheric surface layer has become critically important to scientists working on light propagation studies. Turbulence within the surface layer is a primary factor in determining such phenomena as the intensity of transmitted light when it is received at a point.

Initial experimental efforts to verify turbulence theory predictions were conducted over land. Measurements of wind speed, temperature and humidity in those investigations were taken from a stable platform with auxiliary instrumentation well protected from external weather. Under these conditions relatively accurate measurement of wind speed, temperature and humidity could be performed under a variety of weather conditions.

The marine environment on the other hand presents a number of problems, both in accessibility and platform stability. Protection of equipment and sensors from damaging effects of the ocean environment is also a significant problem. These problems must be solved efficiently if scientists are to achieve reliable analyses and predictions of surface layer phenomena such as momentum transfer and sensible heat transfer.

It is a purpose of this thesis to evaluate the R/V Acania (Figure 1) as an ocean going platform for turbulence and associated profile data collection. The effects of ship's motion and ship's position relative to wind direction (i.e. position of sensors relative to the true wind), and sensor positions on the ship will be considered.

Computation of such turbulent transfer parameters as the drag coefficient, C_D, friction velocity, U_*, and vertical sensible heat flux

Figure 1. The R/V Acania

($\overline{w'T'}$) have been made using data collected aboard the R/V Acania during 1974 and early 1975. The results of these computations will be compared with similar results obtained by Cardone (1969) and Businger et al. (1971). These comparisons will be used as a basis for evaluating the R/V Acania as a platform from which to study turbulence over the ocean.

II. TURBULENCE THEORY

A. GENERAL

Present boundary layer turbulence theory has its basis in the work of Monin and Obukhov (1954). They used a similarity approach to define a representative length scale, L, for the surface layer of the atmosphere,

$$L = - \frac{U_*^3 \, T_0}{\kappa g \, \overline{w'T'}} \quad . \tag{1}$$

Here g is the gravitational acceleration, T is the ambient temperature, and κ is the von Karman constant. The selection of the Monin-Obukhov Length, L, as a stability scaling parameter is based on the assumption that friction velocity, U_*, and vertical heat flux ($\overline{w'T'}$) are constant in the surface layer. Horizontal homogenity within the surface layer is also assumed, and density fluctuations due to pressure changes are neglected.

Monin and Obukhov (1954) applied this scaling length, using dimensional analysis, to the development of a dimensionless function, $\phi_m(z/L)$, which can be used to represent the mean horizontal wind variation with height, $d\overline{U}/dz$, in the surface layer. The following expression is the empirical relationship for the wind shear in their development,

$$\frac{dU}{dz} = \frac{U_*}{\kappa z} \phi_m(z/L) \quad . \tag{2}$$

It can be shown that as vertical turbulent heat flux ($\overline{w'T'}$) decreases to 0, indicating neutral stability, $\phi_m(z/L)$ must approach 1 if Equation (2) is to take on its expected form under neutral conditions.

Assuming that convective mixing is negligible under neutral conditions it follows that for values of $\phi_m(z/L)$ near 1 ($z \ll L$) dynamic turbulence is of primary importance. Thus the absolute magnitude of L becomes an indicator of the vertical extent to which mechanical turbulence controls the turbulent regime.

B. STABILITY CONSIDERATIONS

Observational experiments by Businger et al. (1971) yielded a definite relationship between Richardson Number, Ri,

$$Ri = \frac{g \, (\partial\theta_v/\partial z)}{\overline{\theta} \, (\partial U/\partial z)^2} \quad , \tag{3}$$

and the Monin-Obukhov Length, L, where θ_v is the virtual potential temperature. Figure 2 from Businger et al. (1971) illustrates this relationship quite well. The following expressions are approximations of the relationship between z/L and Ri, proposed by Dyer and Dicks (1970) and Webb (1970) for unstable and stable conditions, respectively,

$$z/L = Ri \quad , \tag{4}$$

$$z/L = \frac{Ri}{1 - \alpha \, Ri} \quad . \tag{5}$$

Here α is an empirically derived constant equal to 0.5.

It is important to note that Businger et al. (1971) observed the Richardson Number to approach a critical value of 0.21 as z/L approached $+\infty$. This suggests that as stability increases, the flow becomes essentially non-turbulent in the surface layer and the effect of mechanical turbulence becomes negligible.

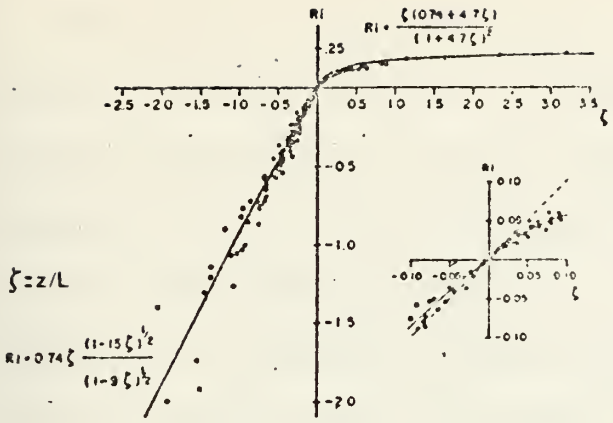

Figure 2. The dependence of Richardson Number on stability.

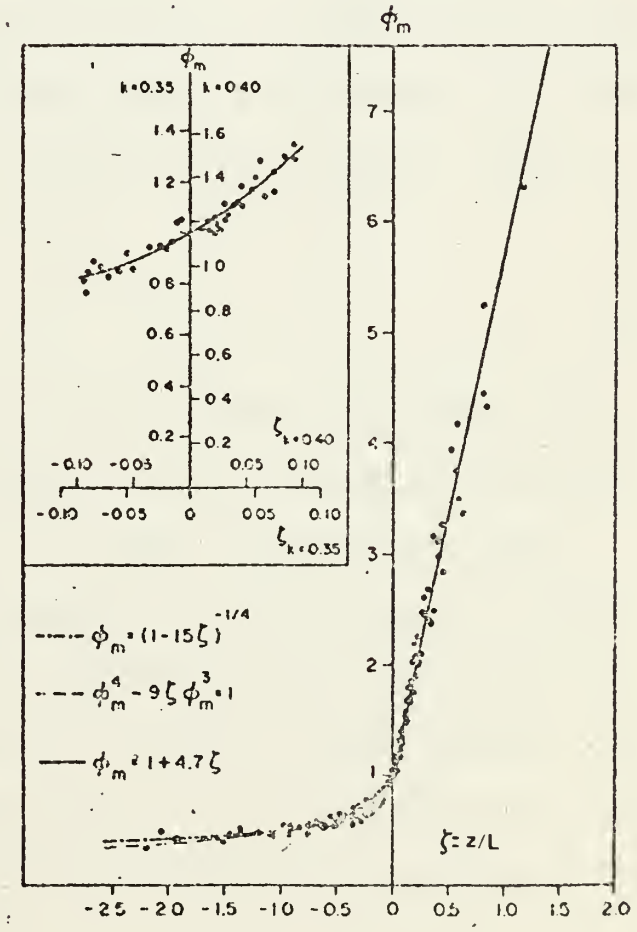

Figure 3. Comparison of dimensionless wind shear observations with interpolation formulae.

The effect of hydrostatic stability on surface layer mechanical turbulence is further illustrated in Figure 3 from Businger et al. (1971). Recalling Equation (2) in light of Figure 3, it becomes apparent that the function $\phi_m(z/L)$ varies relatively little with respect to z/L for unstable conditions approaching a value of 0.5. However, the rapid increase of $\phi_m(z/L)$ as the atmosphere becomes hydrostaticly stable indicates that the neutral assumption breaks down rapidly under increasingly stable conditions. Discussion in the next section will show that the breakdown of the neutral assumption becomes important in the development and use of profiles of wind speed versus Ln(z), for the calculation of the turbulence parameter, U_*, the friction velocity.

C. SURFACE LAYER WIND PROFILES

Monin and Obukhov (1954) and Panofsky et al. (1960) confirmed that under neutral conditions the vertical profile of horizontal wind is logarithmic. Vertical integration of Equation (2) with $\phi_m(z/L)$ equal to 1 yields

$$\overline{U}(z) = \frac{U_*}{\kappa} \mathrm{Ln}(z/z_0) \quad , \tag{6}$$

assuming $\overline{U}_0$ equal to 0. One must realize, however, that both unstable and stable conditions would alter the log profile suggested by Equation (6). Figure 4, from Panofsky et al. (1960) illustrates this effect.

Equation (6) leads to the concept of a surface roughness parameter z_0. This parameter is important in determining the shear stress at the lower boundary of the surface layer. It might be roughly equated to the height of vegetation, for example grass, but it is very difficult to determine accurately. However, z_0 can be eliminated from Equation (6)

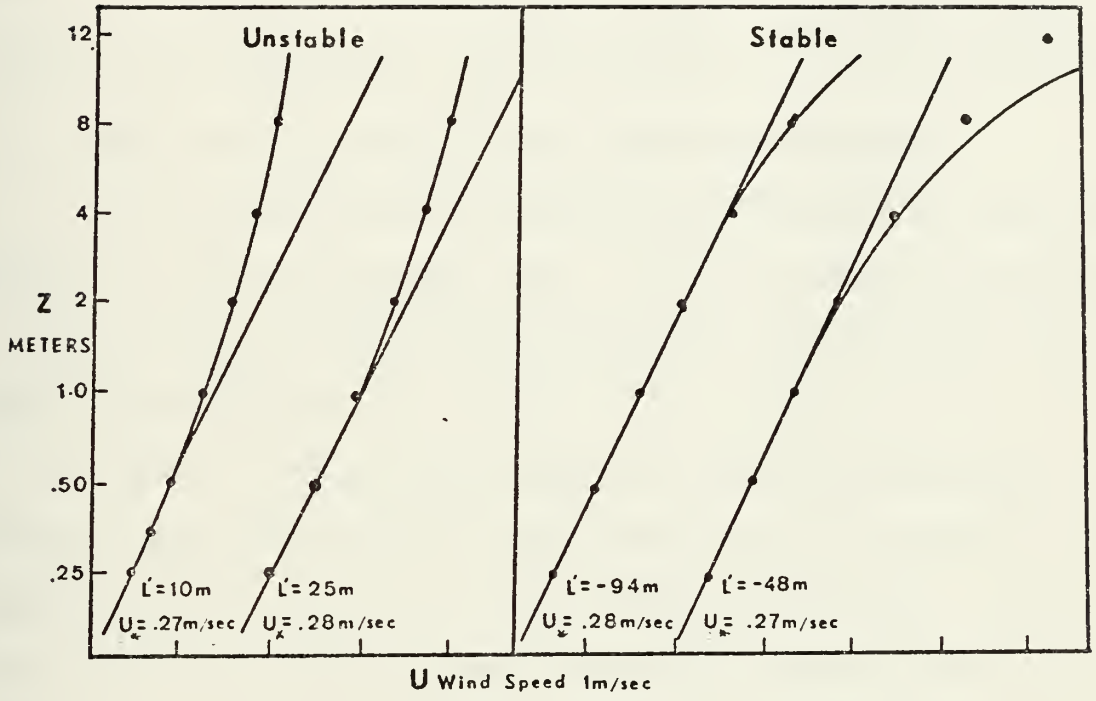

Figure 4. Effects of unstable and stable conditions on height profiles of $\overline{U}$.

by selecting mean winds, $\overline{U}_1$ and $\overline{U}_2$ at 2 levels, z_1 and z_2 such that $(z_1 < z_2)$ and $(z_1 >> z_0)$. Then inserting appropriate values for $\overline{U}_1$ and $\overline{U}_2$, derived from a given wind profile, into Equation (6) and subtracting the two equations will give

$$U_* = \frac{\kappa(\overline{U}_2 - \overline{U}_1)}{\mathrm{Ln}(z_2/z_1)} \quad , \tag{7}$$

where κ is the von Karman constant equal to 0.35. It is important to remember that Equation (7) is only applicable under neutral conditions.

D. CALCULATION OF U_* AND $\overline{w'T'}$ FROM FLUCTUATION PARAMETERS

In the last section U_* was related to the vertical profiles of mean horizontal wind in the surface layer. It is also possible to determine U_* using velocity variance spectra derived from surface layer horizontal wind fluctuation data.

In order to do this it is necessary to have some knowledge of turbulent kinetic energy balance in wave number space. Kolmogorov's second hypothesis plays the key role in developing this knowledge. His hypothesis states that there is a range of energy wave numbers within which Kinetic energy is transferred from one wave number to the next without any dissipation. Within this range of wave numbers, called the inertial sub-range, turbulent kinetic energy dissipation does not occur.

The following relationships were proposed by Kolmogorov to define the spectral wave number region over which his second hypothesis holds:

$$S(k) = C_1 \, \varepsilon^{2/3} \, k^{-5/3} \quad , \tag{8}$$

$$S_T(k) = C_2 C_T^2 k^{-5/3} \quad . \tag{9}$$

Here $S(k)$ and $S_T(k)$ represent the one dimensional spectra of velocity and temperature, respectively, and k is the streamwise wave number. The constants C_1 and C_2 have been empirically determined to be 0.5 and 0.25 respectively. Measurements examined in this study define temporal spectra $S(f)$. The streamwise wave number, k, is related to the temporal frequency, f, by

$$k = \frac{2\pi f}{\bar{U}} \quad , \tag{10}$$

where $\bar{U}$ is the mean wind at the measurement level. This is based on Taylor's (1938) "frozen turbulence" hypothesis, The term "frozen" implies that the turbulence pattern remains unchanged as it sweeps past the probe.

Of interest in this study is, ε, the viscous molecular turbulent kinetic energy dissipation. Solving Equation (8) for ε produces

$$\varepsilon = \left(\frac{S(k)k^{5/3}\cdot 3/2}{C_1}\right) \quad . \tag{11}$$

Under neutral conditions it has been shown that turbulent kinetic energy production is equal to the rate of molecular dissipation of turbulent kinetic energy, ε, hence

$$\varepsilon = U_*^2 \frac{\partial \bar{U}}{\partial z} \quad . \tag{12}$$

Combining Equation (2) for a neutral condition, $\phi_m(z/L) = 1$, with Equation (12) and solving for U_* gives

$$U_* = (\varepsilon \kappa z)^{1/3} \quad , \tag{13}$$

where κ is von Karman's constant. Thus, under neutral conditions, U_* can be estimated from either mean wind profiles using Equation (7) or from fluctuation data using Equation (13).

It is also possible to determine the vertical sensible heat flux ($\overline{w'T'}$) from measurements of wind and temperature fluctuations and vertical temperature gradient. Corrsin (1951) proposed the following relationship for the temperature structure parameter C_T^2:

$$C_T^2 = 3.2\ N\ \varepsilon^{-1/3} \quad , \tag{14}$$

Here ε has been previously defined and N is the dissipation rate of temperature variance given by

$$N = \overline{w'T'}\ \partial\theta/\partial z \quad . \tag{15}$$

on the basis of the temperature variance balance, where θ is the potential temperature. Hence, combining Equations (14) and (15) and solving for $\overline{w'T'}$ yields

$$\overline{w'T'} = \frac{C_T^2\ \varepsilon^{1/3}}{3.2\ \partial\theta/\partial z} \quad . \tag{16}$$

E. THE BULK AERODYNAMIC METHOD

One of the comparisons used in this study to evaluate estimates of vertical heat flux ($\overline{w'T'}$) in the surface layer was based on work done by Friehe (1976). Friehe's results feature the use of bulk aerodynamic formulae to estimate surface layer heat and moisture fluxes. He used a great deal of data from "platforms of opportunity" for these estimates. The bulk formulae are necessary because data from these platforms usually consist of mean wind and temperature measured at only one level and a sea surface temperature.

The bulk aerodynamic expression for the vertical sensible heat flux is as follows:

$$\overline{w'T'} = C_H \, \overline{U}_1 \, (\overline{T}_S - \overline{T}_1) \quad . \tag{17}$$

Here C_H is a heat transfer coefficient constant for the given height z_1 while $\overline{U}_1$ (m/sec) and $\overline{T}_1$ (°C) are the mean wind and temperature at z_1 and $\overline{T}_S$ is the surface temperature. Friehe also considered the stability influence on C_H by defining it as follows (for 10 meters):

$$C_H = 1.46 \times 10^{-3} \quad (\overline{U} \, \Delta \, T > 25 \text{ m/sec}) \, ,$$

or

$$C_H = 0.91 \times 10^{-3} \quad (\overline{U} \, \Delta \, T < 25 \text{ m/sec}) \, .$$

In Friehe's investigation z_1 was 10 meters.

The next step in Friehe's study was to derive an expression for z/L using the bulk aerodynamic expressions for the flux terms in L. He

derived the following expression for 1/L:

$$L^{-1} = -\frac{\kappa g}{C_D}\left(\frac{C_H \Delta T}{\overline{T}_v \overline{U}_{10}} + \frac{0.61 \times 10^{-3} C_E \Delta Q}{\overline{U}_{10}^2}\right) \quad . \tag{18}$$

In Equation (18) C_D is the drag coefficient at 10 meters equal to 1.32×10^{-3}, C_E is the moisture transfer coefficient equal to 1.3×10^{-3}, and C_H is the heat transfer coefficient discussed earlier in this section. Also ΔQ (gm/m^3) is the moisture difference and $\Delta\overline{T}$ (°C) is the temperature difference between the surface and 10 meters, and $\overline{T}_v$ is the surface mean ambient virtual temperature.

F. THE DRAG COEFFICIENT

Having determined values for U_* it is possible to calculate a momentum drag coefficient, C_D, that is constant at any given height in the surface layer. The drag coefficient is related to U_* and the mean wind at a given level z_1 by the expression

$$C_{D1} = \frac{U_*^2}{\overline{U}_1^2} \quad . \tag{19}$$

Many studies have been conducted to determine a representive value of C_D at 10 meters (e.g. Cardone 1969). Cardone's summary of C_{10} versus wind speed for the results of several investigations is presented in Figure 5. Calculation of C_{10} employing U_* determined from both mean wind profiles and dissipation rates, when plotted against mean wind at 10 meters, can be used to evaluate wind observations made aboard the R/V Acania.

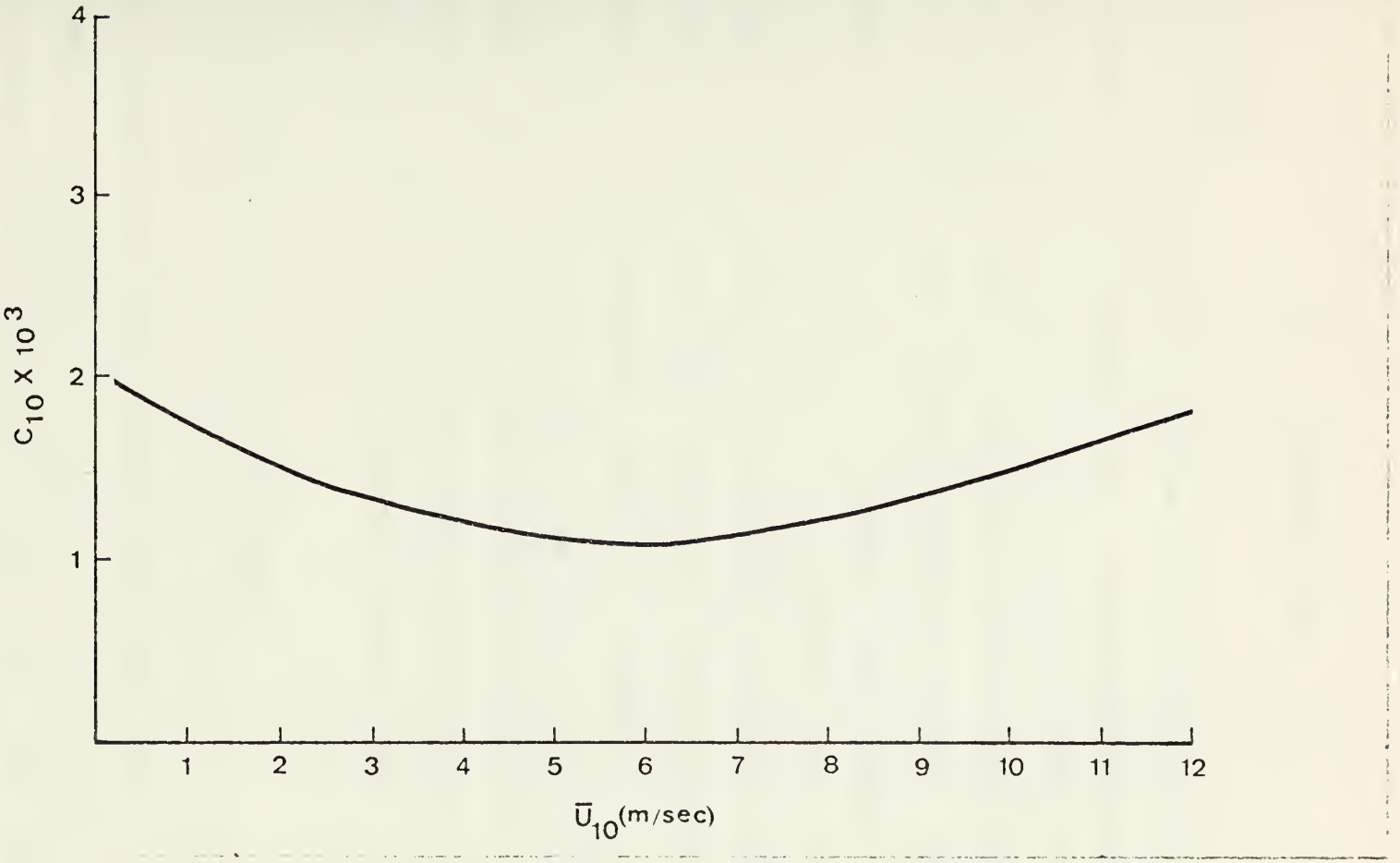

Figure 5. Plot of ten meter drag coefficient, C_{10}, against mean wind speed at ten meters from Cardone (1969).

III. DATA COLLECTION

A. PLATFORM

All data was collected aboard the R/V Acania while anchored in about 30 fathoms of water in Monterey Bay. The ship's anchorage position, shown in Figure 6, lies about 4000 yards northeast of Point Pinos on a line between Point Pinos and the Holiday Inn on Del Monte Beach. The R/V Acania is 48.4 meters long with a beam of 6.5 meters. She displaces 224 metric tons with a draft of 2.7 meters. Figure 7 shows exact position of the towers which support the instrumentation and it shows length of cable runs and position of the processing and recording equipment.

While anchored, the ship's engines were used as necessary to maintain ship's head into the wind. This led, on occasion, to placing the ship at an angle to the seas, thus exaggerating roll and pitch of the platform. Also, turning the screws during data collection probably affected the sea surface temperature sensor which was placed next to the ship at the after end of the deckhouse on the port side in the vicinity of the port screw.

B. INSTRUMENTATION AND PROCESSING EQUIPMENT

Table I lists the data periods used in this study and indicates which instrument levels were operable during each period.

Mean wind measurements were obtained with Thornthwaite Associates cup anemometer wind profile register systems model 104 as shown in Figure 8. When rotating, the slotted shaft of the anemometer serves as a shutter between a light source and a photoelectric cell. Three cups are mounted on stainless steel tubes attached to the main shaft at 120° intervals. One of these units was placed at each of 4 levels as indicated in

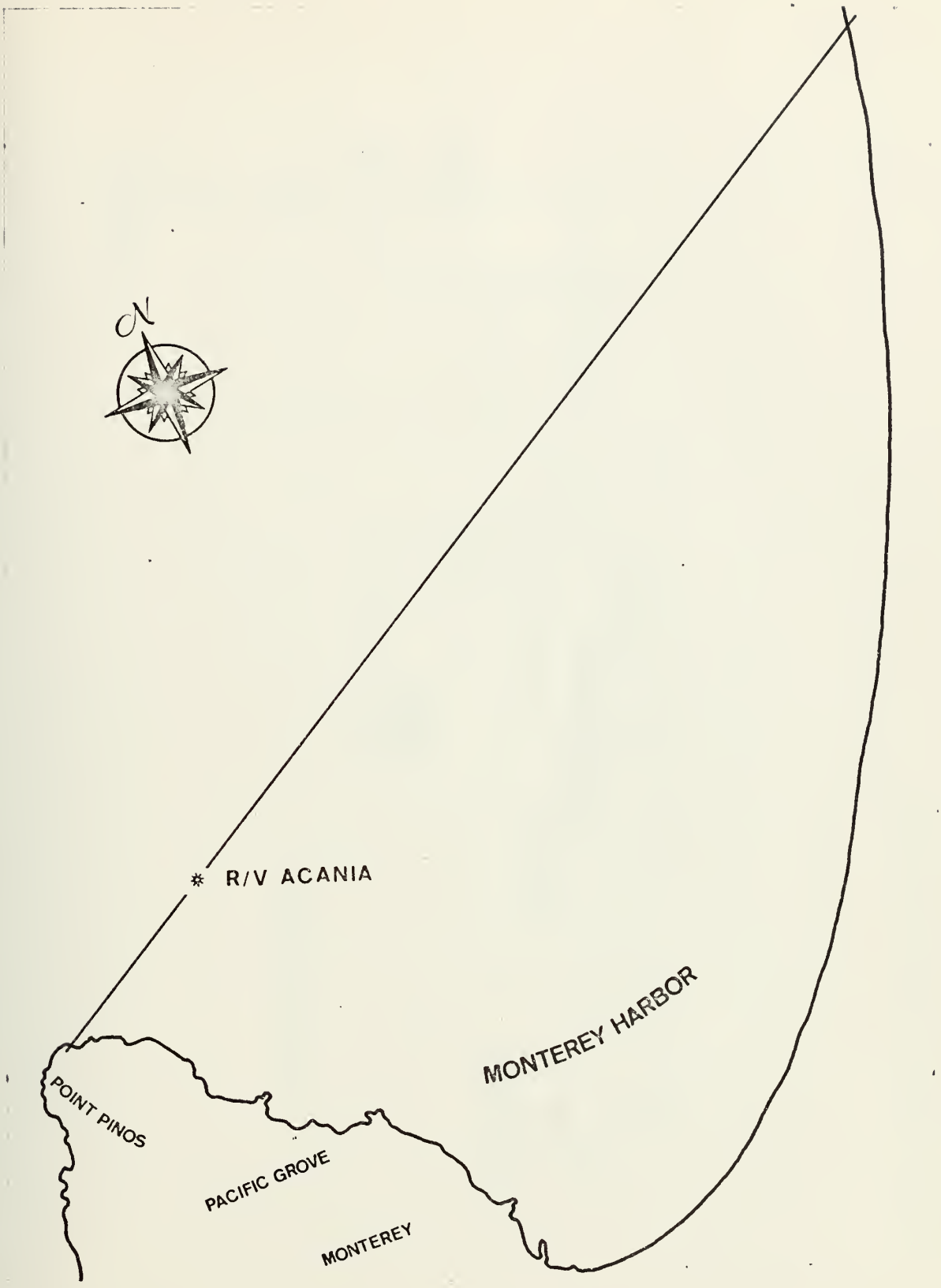

Figure 6. The R/V Acania anchorage position.

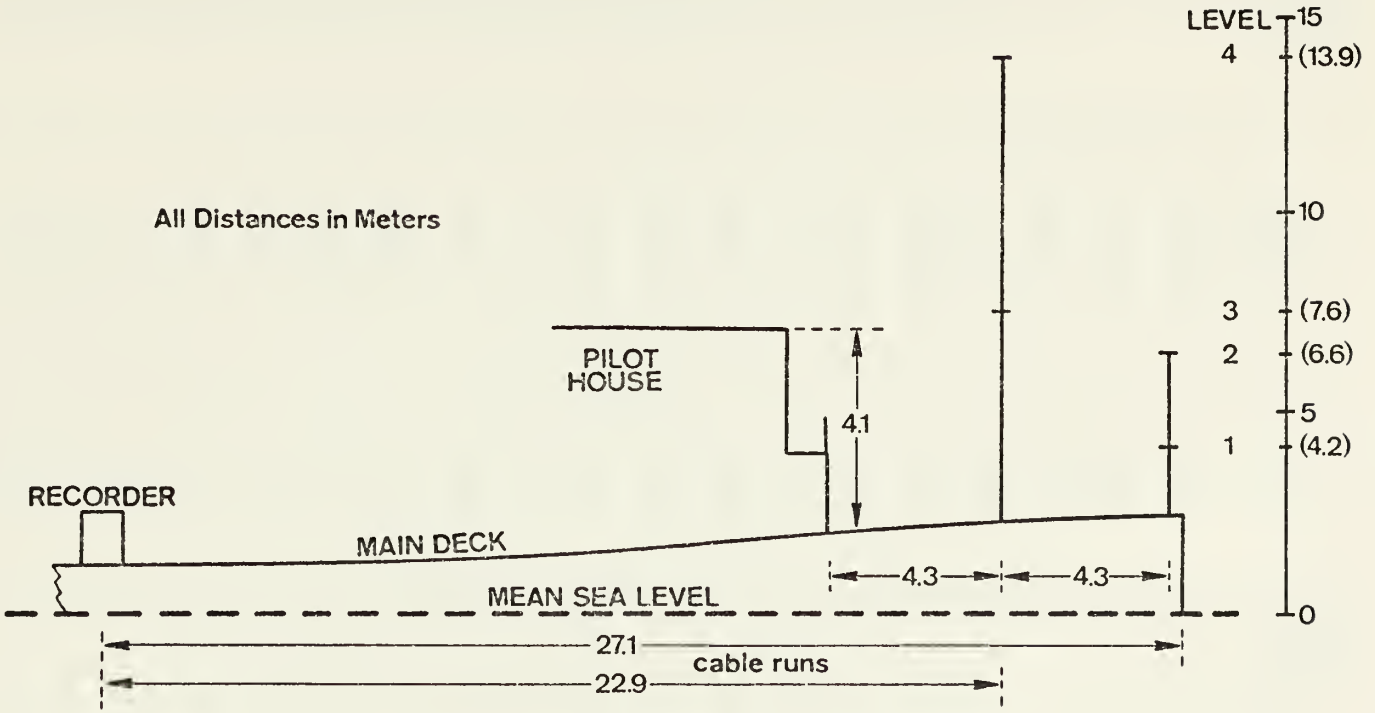

Figure 7. Sensor location on board R/V Acania.

TABLE I

*PERIOD NUMBER	DATE	TIME	WIND LEVEL +,a	TEMPERATURE LEVEL +,a
1	3/27/74	1841	1	4
2	3/27/74	1902	1	4
3	3/27/74	1928	1	4
4	3/27/74	2117	1	4
5	3/28/74	1902	2	4
6	3/28/74	2059	2	4
7	8/13/74	1700	2	4
8	8/13/74	1742	2	4
9	8/13/74	1742	2	4
10	9/18/74	1643	2	4
11	9/19/74	1735	2	4
12	9/19/74	1846	2	4
13	9/19/74	1900	2	4
14	9/19/74	1929	2	4
15	9/19/74	2011	2	4
16	9/19/74	2115	2	4
17	9/19/74	2158	2	4
18	9/19/74	2243	2	4
19	9/20/74	0014	2	4
20	9/20/74	0056	2	4
21	9/20/74	0140	2	4
22	9/20/74	0530	2	4
23	9/20/74	0552	2	4

TABLE I (continued)

*PERIOD NUMBER	DATE	TIME	WIND LEVEL +,a	TEMPERATURE LEVEL +,a
24	11/21/74	1800	2	4
25	11/21/74	1821	2	4
26	11/21/74	1842	2	4
27	11/21/74	1903	2	4
28	11/21/74	2027	2	4
29	11/21/74	2048	2	4
30	11/21/74	2109	2	4
31	11/21/74	2130	2	4
32	3/27/75	1502	2	4
33	3/27/75	1519	2	4
34	3/27/75	1539	2	4
35	3/27/75	1600	2	4
36	3/27/75	1644	2	4
37	3/27/75	1656	2	4
38	3/27/75	1956	3	4
39	3/27/75	2020	3	4
40	3/27/75	2045	3	4
41	3/27/75	2106	3	4

* Hereafter period numbers will be referred to in place of date and time.

+ Refer to Figure 7 for instrument level locations.

a 1 = Levels 2, 3, 4
2 = Levels 1, 2, 3, 4
3 = Levels 1, 2, 3
4 = Levels 0, 1, 2, 3, 4

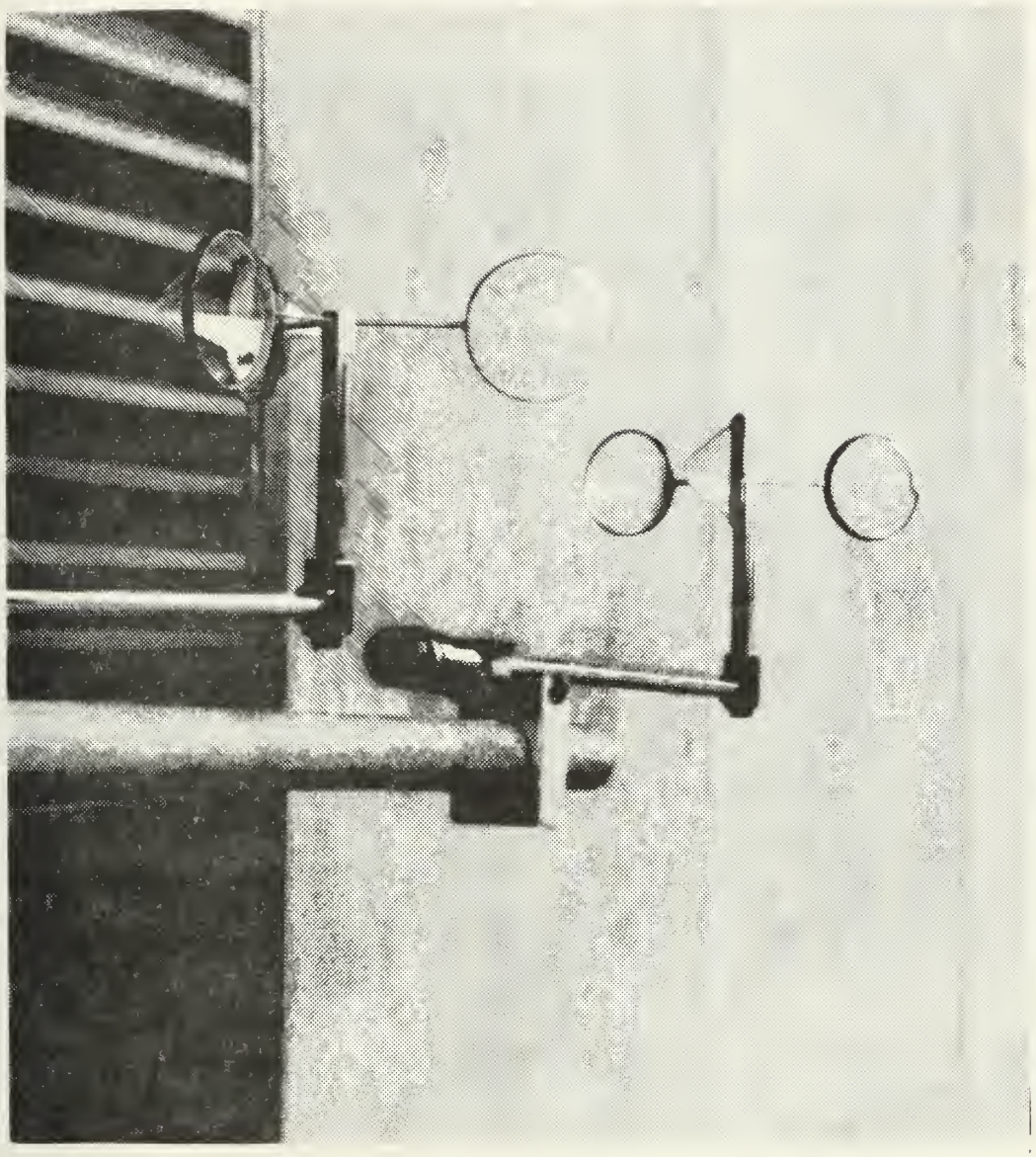

Figure 8. C.W. Thornthwaite Anemometer Cups.

Figure 7. Each was connected to the after deckhouse laboratory by an individual coaxial cable, as were all sensors mounted on the 2 towers.

Placement of the after tower could be a problem. Noting from Figure 7 the position of the after tower relative to the deckhouse structure, it is reasonable to assume that turbulence created by the deckhouse might affect at least the third sensor level.

Data logging for the mean system was accomplished using an NPS developed micro-processor based data acquisition system. This MIDAS (Microprogrammable Integrated Data Acquisition System) utilizes an Intel 8008 central processor to control the sampling, averaging, and recording of mean meteorological data. All software programming is written in PL/M to facilitate the writing of a self-documenting program.

The operator is interfaced with the system via teletype for full duplex input/output communications and program control over the sample start-time and the number of samples to be averaged before outputting. The operator may also alter the present preset sample list by adding or deleting various sensors as they come on line or become inoperable. Once initiated, the system is fully automated to sample the tailored list of sensors every 30 seconds and periodically print output values averaged over the selected interval of from one minute to one hour. In this study a ten minute averaging period was used.

Output values are printed out on the teletype in columnized format with the time of print as a leader. The teletype has a paper tape punch incorporated which may be activated by the operator to produce a data copy concurrent with the print-out. A magnetic cassette tape recorder has been integrated into the system as a third data output device. It

is planned to interface this cassette to an HP 9830 portable computer so that profile and gradient flux estimates can be performed on board automatically using the BASIC programming capability of the HP 9830. Presently, data cards are punched from the paper tape output and processed on the IBM 360 system at NPS.

Velocity fluctuation measurements were performed using TSI model 1210 probes with sliding support shields and tungsten wires. The shields permitted isolation of the sensing area for the determination of the undisturbed velocity, v_o, before and after each experiment. The platinum coated tungsten wire was small enough to resolve the viscous dissipation scale without any need to apply wire length corrections. The wire was fitted with plated ends for isolating the sensing area and thereby minimizing flow disturbance.

Electronics associated with each probe were a TSI Model 1054B linearized anemometer and a TSI Model 1056 variable decade module. The anemometer had a linear frequency response from DC to 10 KHz and the variable decade module operated with a 0-60 ohm range.

Sensor placement required exceptionally long cable runs, but any decrease in system frequency response had little effect in the frequency band of interest.

Temperature fluctuations were measured using similar sensors. The only difference was that a platinum wire was used in place of tungsten. The temperature fluctuation system was designed for a resolution of 0.001°C at frequencies up to 1KHz.

The temperature fluctuations were measured using a bridge developed by personnel at GTE Sylvania, the GTE Sylvania Model 140. The system was slightly modified for use aboard the R/V Acania.

The baseband portion of this system is basically a balanced wheatstone bridge excited by a 3 KHz signal with a synchronous detector on the output. Segments of a very small diameter platinum wire serve as temperature sensors in opposite arms of the bridge. The resistance temperature coefficients result in an output from the bridge which is proportional to the temperature difference between the two probes.

The sensor wire is 0.5 centimeters long and 2.5×10^{-4} centimeters in diameter. This extremely small mass allows a response to temperature variations of up to 1 KHz, while electronic amplification allows temperature differences as small as 0.004°C to be observed.

Both wind and temperature fluctuation data are recorded on a Sanborn Model 3950 fourteen channel tape recorder. Real time readout on an eight channel chart recorder, Brush Model 240, was used to check the quality of the signals coming from the sensors. The charts were also used to select the periods to be analyzed for this study.

Hewlett Packard model HP-2850 temperature sensitive quartz crystal probes (Figure 9) were used to obtain mean temperature at the sea surface and 4 tower levels. The RF signal from the probes and a reference oscillator were mixed in a Hewlett Packard HP-2801A readout unit to produce a beat frequency whose signature can be analyzed to within 0.001 degrees centigrade per hertz. Each sensor received pre-experiment calibration against a platinum resistance wire thermometer in a temperature controlled circulating water bath. It was checked over the range of expected temperatures. The accuracy in achieving a .005 degree centigrade correction factor was a constant for each probe. The tower mounted sensors were housed in an aspirated shelter shown in Figure 9 to eliminate radiation effects.

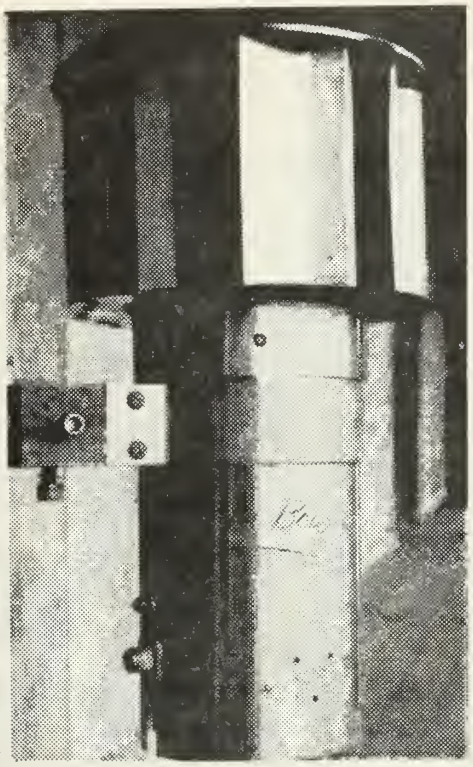

A.

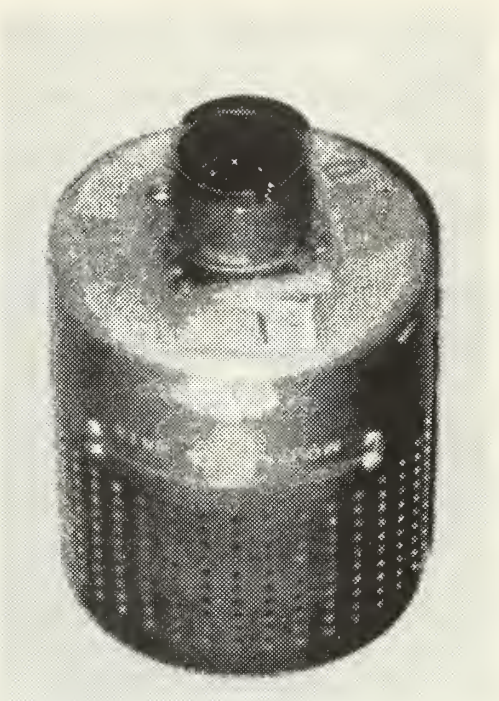

B.

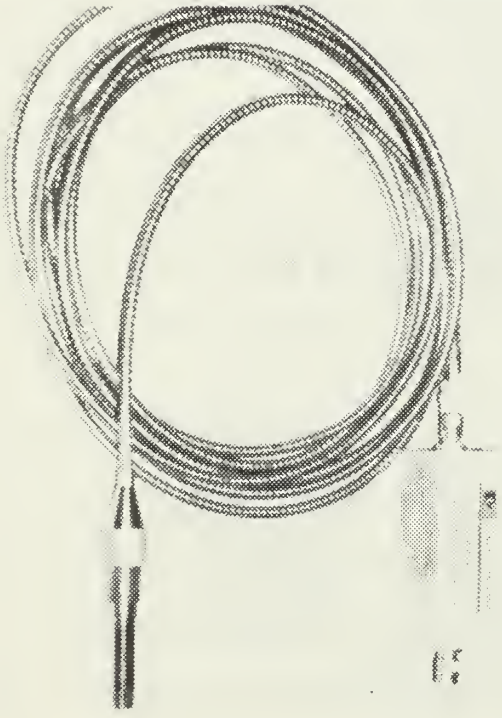

C.

Figure 9.

A) C.C. Breidert Company Air-X-Houster Shelter.
B) Dunmore-type Lithium Chloride Sensor.
C) Quartz Thermometer Probe.

It is felt that placement of the sea surface temperature sensor near the side of the ship could have caused erroneous surface temperatures due to radiation effects near the hull and mixing effects from the screws which were sometimes used to maintain ship's position during the experiments. The recent movement of this sensor to a position forward of the bow should make further sea surface temperature data more reliable.

Mean relative humidity information was obtained using Dunmore-type lithium chloride sensors (Figure 9). This sensor was also placed in the aspirated shelter. The basic principle of operation of this sensor is resistance change in an electrolytic solution generating a reference voltage variance proportional to the relative humidity change. Automatic temperature compensation in the instruments meet the following specifications for relative humidity:

$\pm$3% humidity below 90% and

$\pm$4% relative humidity above 90%.

Sensor calibration was accomplished by a comparative method using a saturated saline solution in a closed container.

C. SPECTRUM ANALYSIS AND INTERPRETATION

Spectrum analysis is the process through which wind fluctuation data is converted to a turbulent energy density spectrum. Appropriate 21 minute segments of data recorded on magnetic tape were transmitted to a Federal Scientific Model UA-500-1 Spectrum Analyzer-Averager. Figure 10 pictures the analyzer while Figure 11 is a block diagram of the analysis process.

Procedures for converting velocity spectral values, obtained with

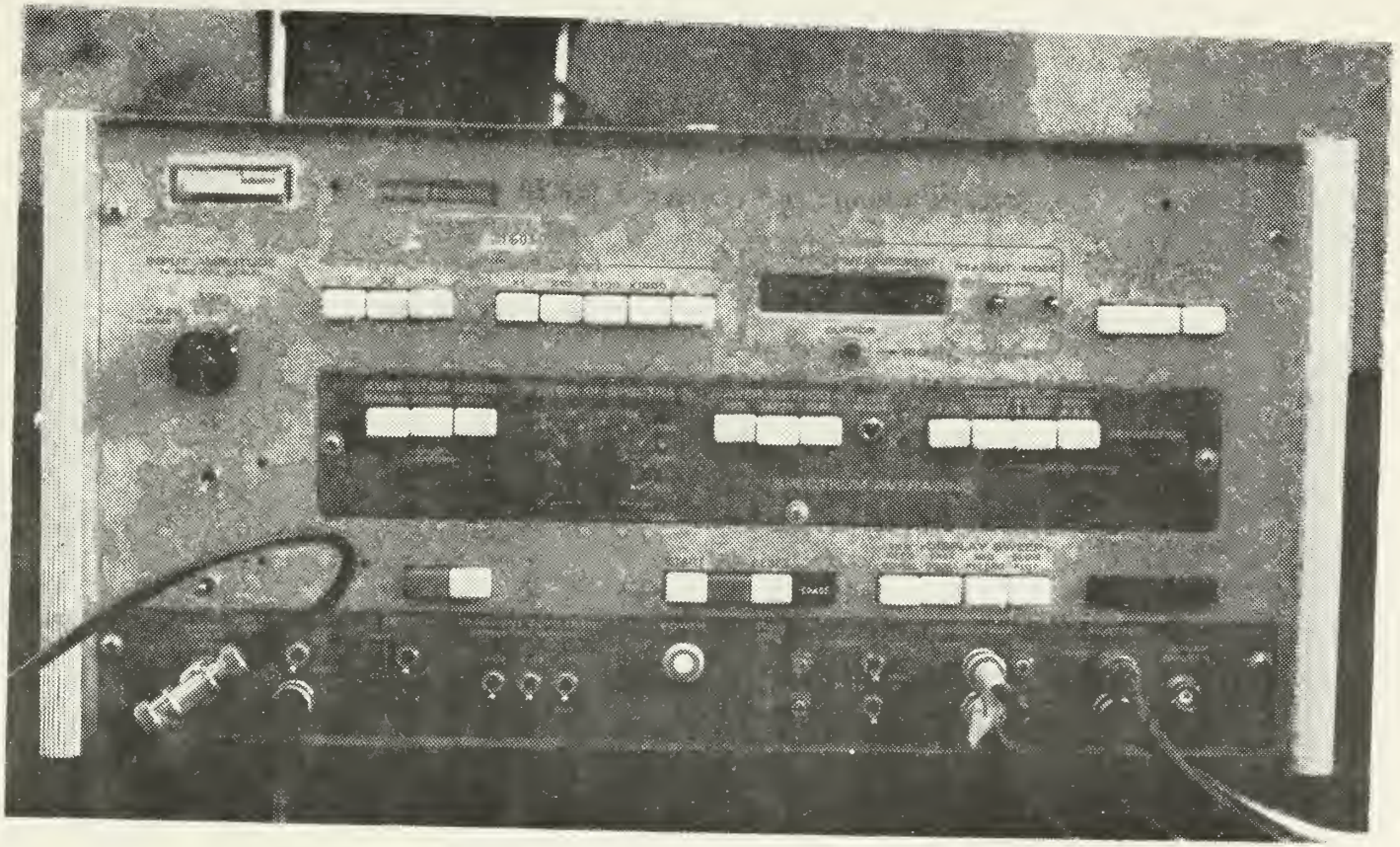

Figure 10. Federal Scientific Model UA-500-1 Spectrum Analyzer-Averager.

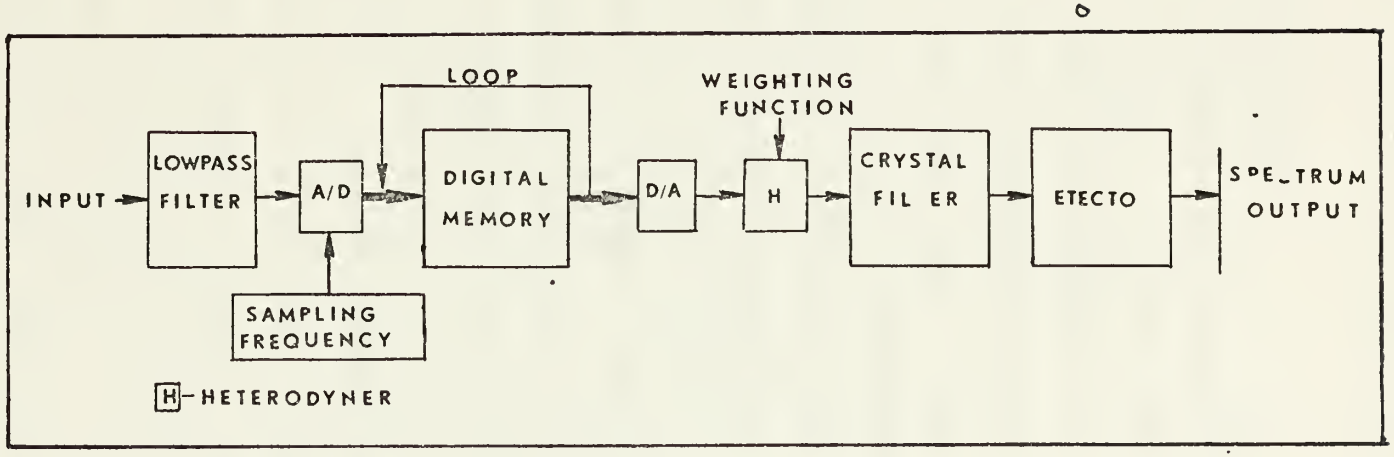

Figure 11. Block diagram of spectrum analyzer.

an analog spectrum analyzer, to engineering units and for obtaining the turbulence parameter ε from the velocity spectra are described in this section. A parallel discussion for temperature spectra appears in Hughes (1976).

1. Spectral Plot Scaling

A necessary procedure was to scale the spectral plots to relate RMS input voltages to power spectral densities; variance per unit frequency. To obtain power spectral density levels, corresponding to RMS voltage inputs, calibrated scale charts had to be constructed.

The charts were constructed as follows. Amplitude scaling was accomplished by using an externally generated signal whose RMS value was determined by an RMS meter. Using a 0-db (.1v) input and a spectral gain of 0-db(x1), a signal with amplitude equal to 0.1 volts RMS was produced on a screen display as a spike near the selected frequency. This spike was then plotted with an X-Y plotter. Successively, the input gain was stepped down to attenuate the amplitude of the input signal by 10db increments, and plots of the height of each resulting spectral spike (amplitude) were then added to the X-Y plot, at different frequencies. These plots represented a graduation of RMS input from a minimum of 0.001 volts RMS to a maximum of 0.1 volts RMS. An example of such a calibration plot on the chart appears in Figure 12. These procedures were performed regularly during analyses to insure continual calibration of the spectrum analyzer and X-Y plotter.

For purposes of the chart format the RMS voltages were converted to LOG 10 units and a graduated scale was constructed so that the logarithm of volts RMS could be interpolated from spectral plots. The amplitude scale was adjusted for each spectrum as a function of both

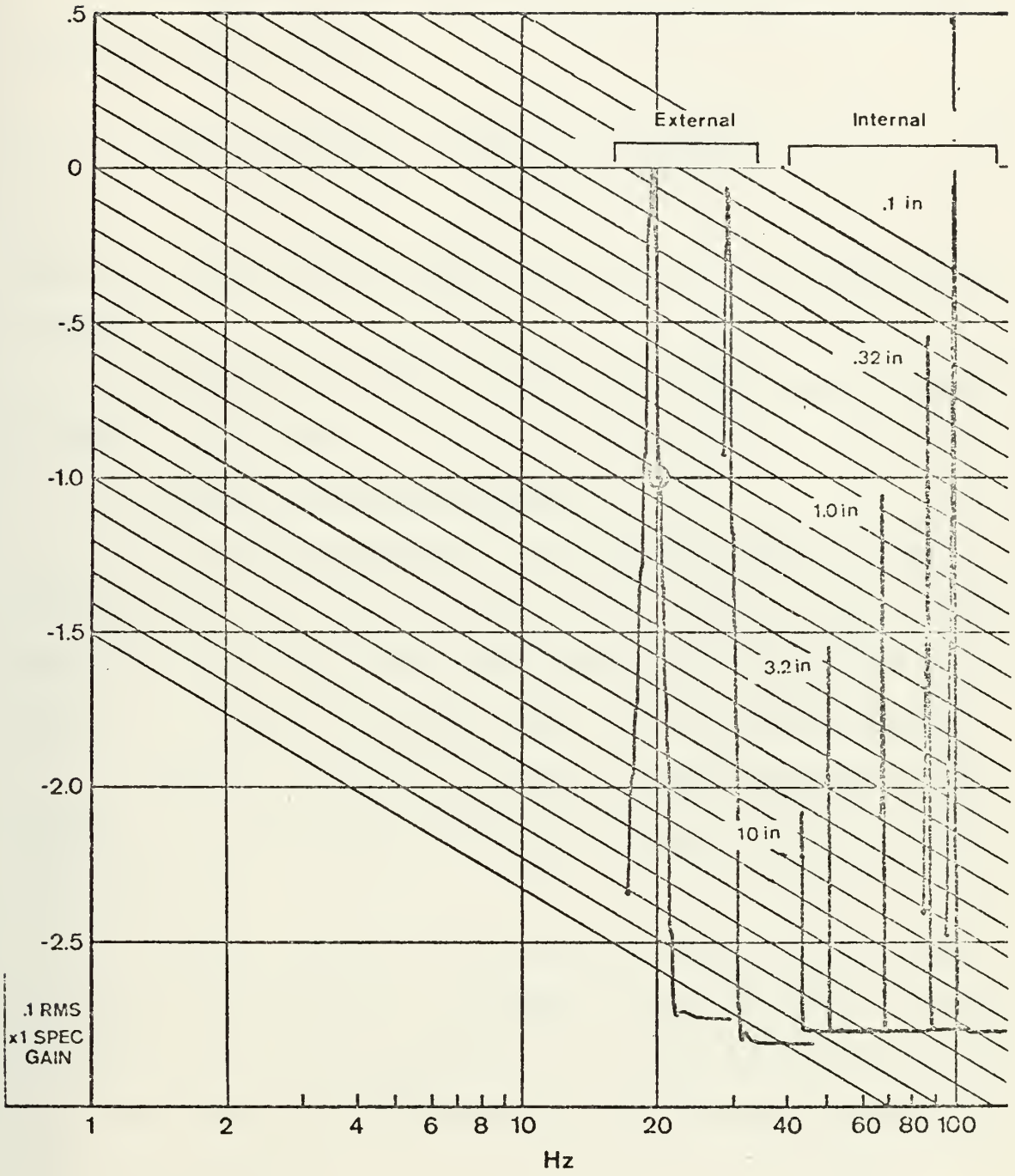

Figure 12. Calibration plot for spectrum analyzer.

input gain and spectral gain. These values were then converted to PSD levels for use in calculating ε values.

The equation (based on Federal Scientific specifications) to convert volts RMS to PSD is

$$\text{PSD level } (V^2/\text{Hz}) = \frac{0.79(\text{cal. level } V_{RMS})^2}{\text{Filter Bandwidth}} \tag{20}$$

where the filter bandwidth, β=0.4, is a function of the analysis range selected.

A more detailed explanation of the spectrum analysis process can be found in Lund (1975).

2. Obtaining ε From Scaled Spectra

The turbulence parameter, ε, was obtained from the scaled variance spectra on the basis of the universal formula, Equation (8), for the inertial sub-range in wave number space S(k). This expression predicts a -5/3 slope for the spectra when plotted in log-log formats.

Figures 13, 14, and 15 are typical spectra considered in the analyses. It is noted that velocity variance spectra have consistent -5/3 slopes.

Assuming -5/3 slopes for the variance spectra, the intercept of the -5/3 slope with the 1 Hz frequency line was the spectral density, denoted PSD, value used in computing ε. The measured PSD value obtained from velocity spectra was converted to a spectral density in engineering units by the equation

$$\begin{aligned} S(f) &= C^2 \times \text{PSD} \\ &= (\text{cm/sec/volt})^2 \times \text{volt}^2/\text{Hz} = (\text{cm/sec})^2/\text{Hz} \end{aligned} \tag{21}$$

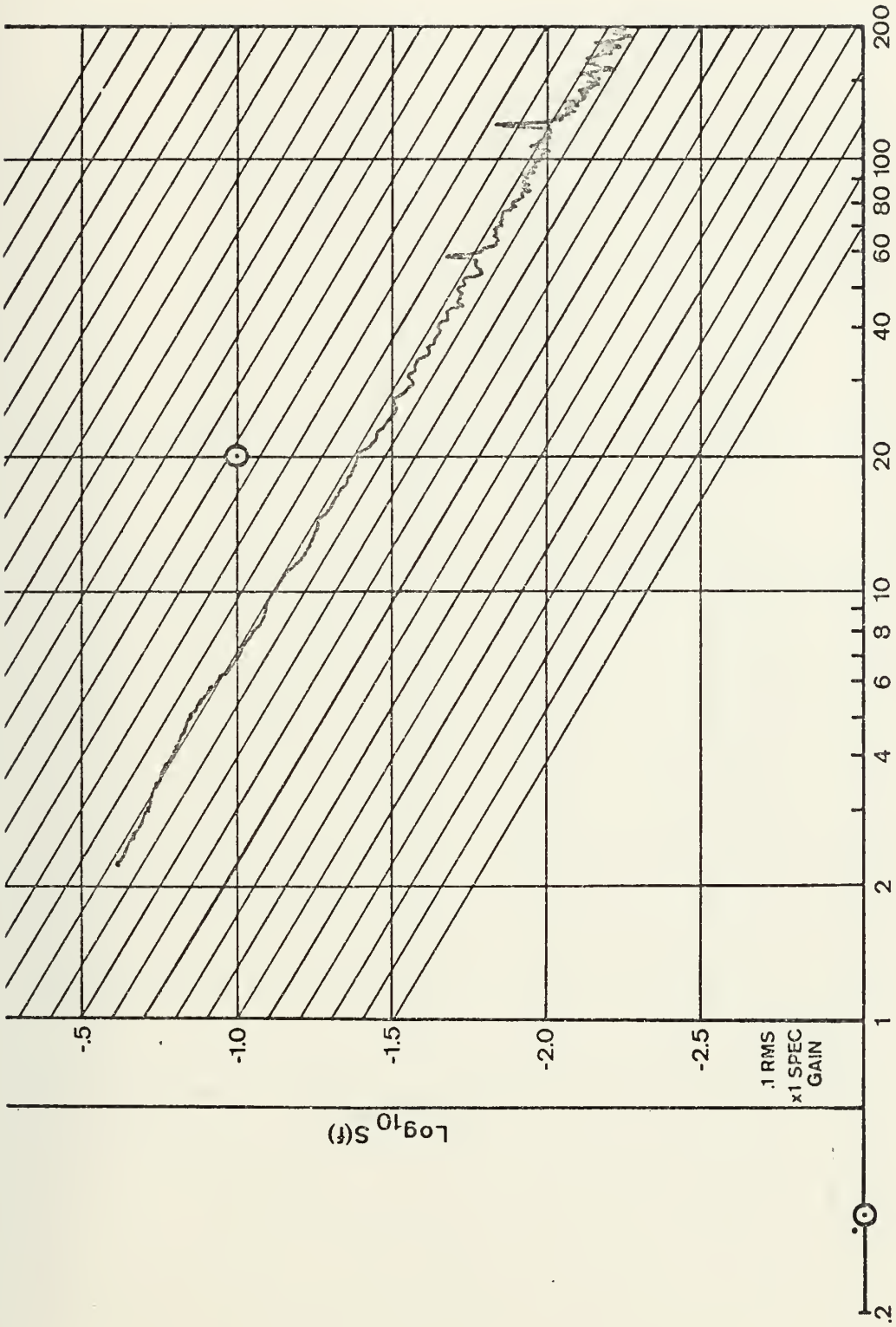

Figure 13. Typical velocity spectrum with distinct -5/3 slope. Plotter calibration points are shown as circles with dots in the center.

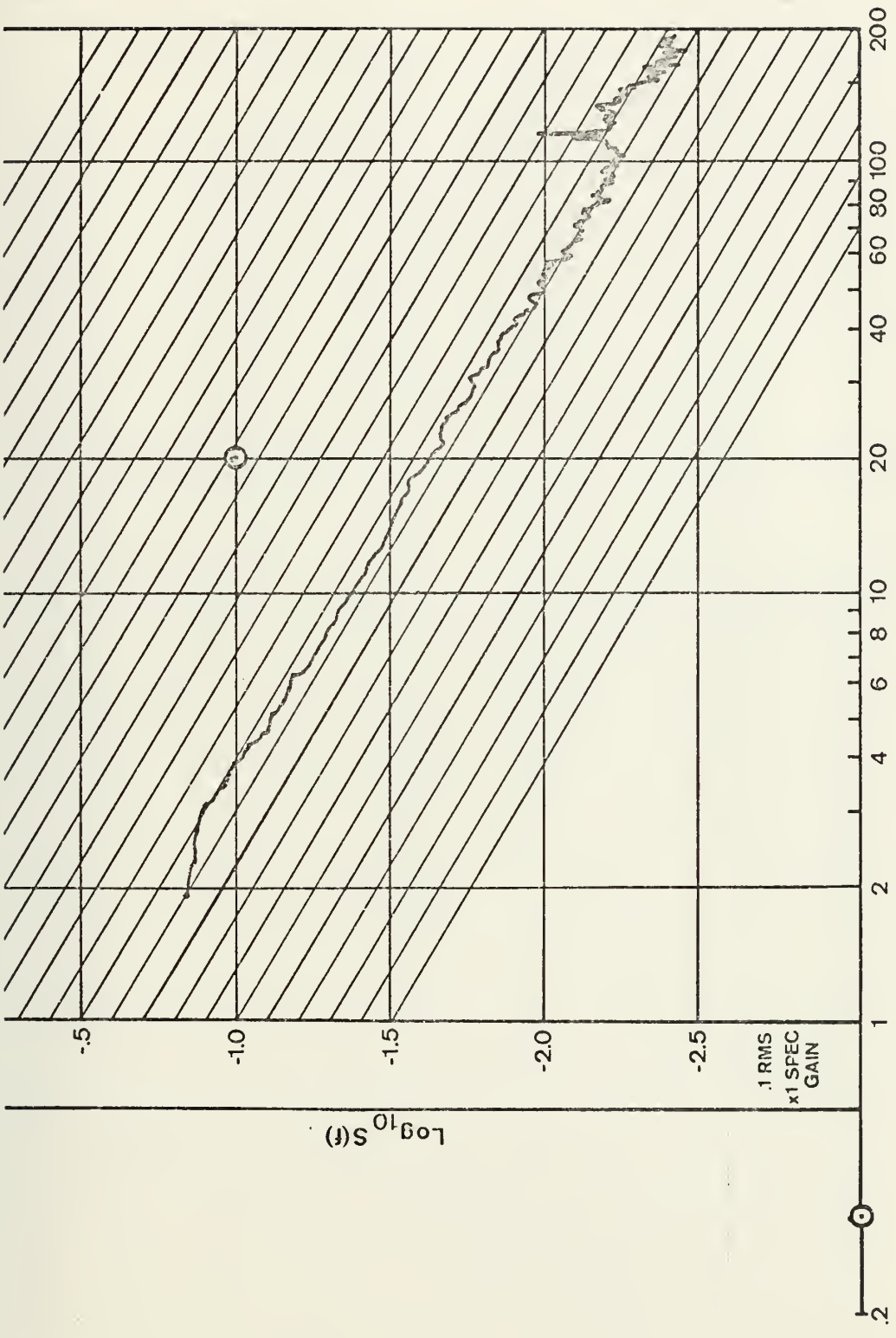

Figure 14. Typical velocity spectrum with distinct -5/3 slope.

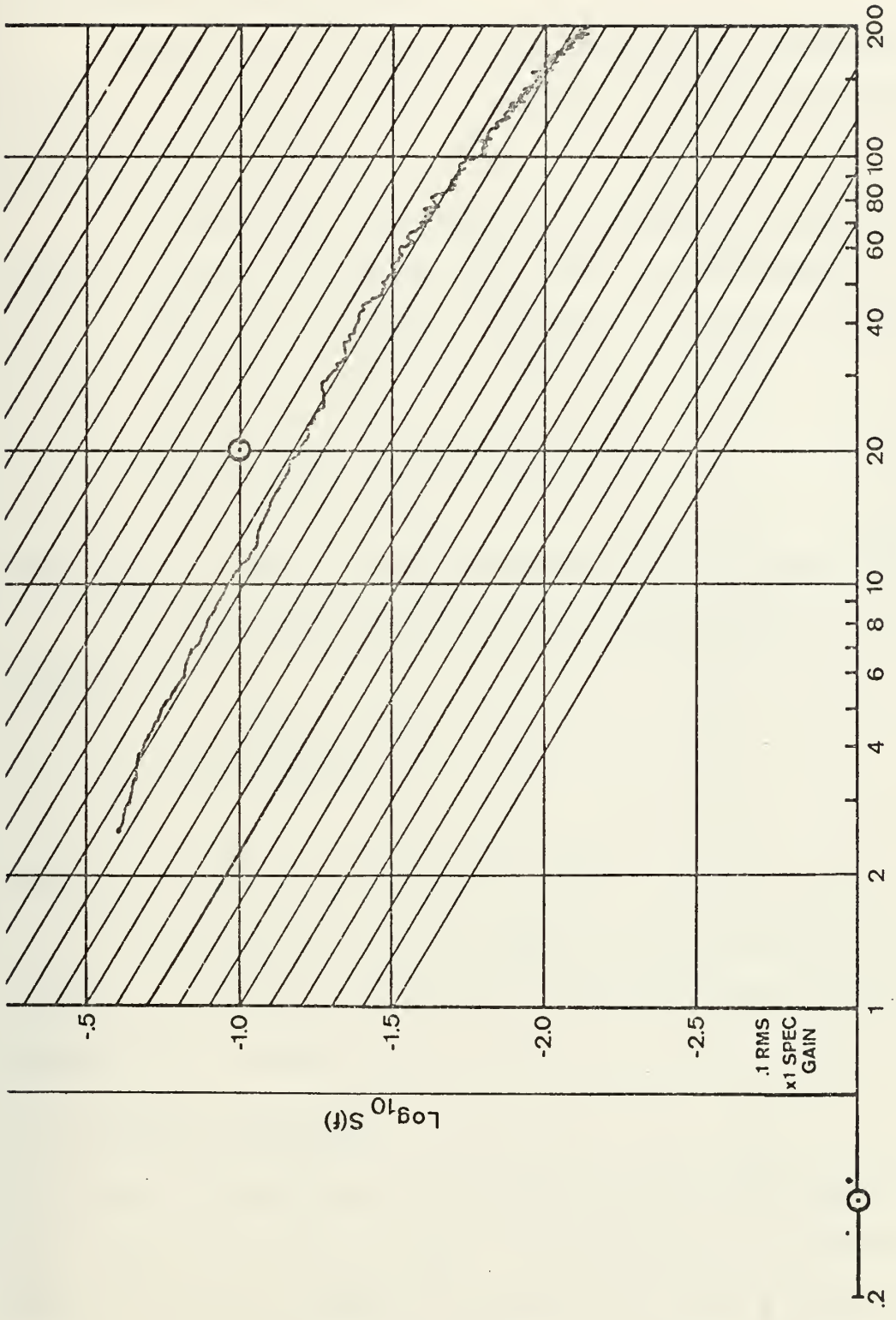

Figure 15. Velocity spectrum lacking distinct -5/3 slope.

where C is the hot-wire calibration factor, the determination of which is discussed in the next section.

Since velocity fluctuations were measured at a fixed point in the flow, the resultant spectra are realized at a "temporal" frequency, f, and correspond to S(f).

To obtain an ε, the temporal, f, and space, k, scales must be related in order to use Equation (8). This is accomplished by using Taylor's (1938) "frozen turbulence" hypothesis presented in Section II.D. of this study. Thus Equation (8) can also be written as

$$fS(f) = kS(k) = C_1 \varepsilon^{2/3} k^{-2/3} \tag{22}$$

where S(f) is a spectral density value with units of $(Cm/sec)^2/Hz$.

The final form of Equation (22) relating ε to S(f), which is measured, is

$$\varepsilon = \left(\frac{k^{2/3} fS(f)}{C_1}\right)^{3/2} \tag{23}$$

where, empirically, $C_1 = 0.25$ and $k = 2\pi f/\bar{U}$.

From Equation (23), with measured f, S(f), and $\bar{U}$, ε can be determined at each level of interest. This was the final form used to determine the ε values.

D. HOT WIRE CALIBRATION

In-situ calibrations of the velocity sensors were accomplished several times during each experiment. In this procedure recordings were made of both the cup anemometer indicated wind speed and the corresponding hot wire voltage output. The sensor wind speed is given by,

$$v^2 = a\,\bar{U}^{1/2} + b, \tag{24}$$

where v is the voltage and $\bar{U}$ is the mean wind speed for any given level. The constants, a and b, are calibration curve slope and intercept respectively, obtained from the in-situ calibration.

To convert the power spectral density levels to velocity units requires a calibration factor given by

$$u' = Cv' \tag{25}$$

where C is the calibration factor in cm/sec/volt, v, is the voltage fluctuation and u' is the velocity fluctuation. Differentiating Equation (24) yields

$$u' = \left(\frac{4v\,\bar{U}^{1/2}}{a}\right)v' \ , \tag{26}$$

which when substituted in Equation (25) gives

$$C = \frac{4v\,\bar{U}^{1/2}}{a} \ . \tag{27}$$

Figure 16 is a sample in-situ calibration curve.

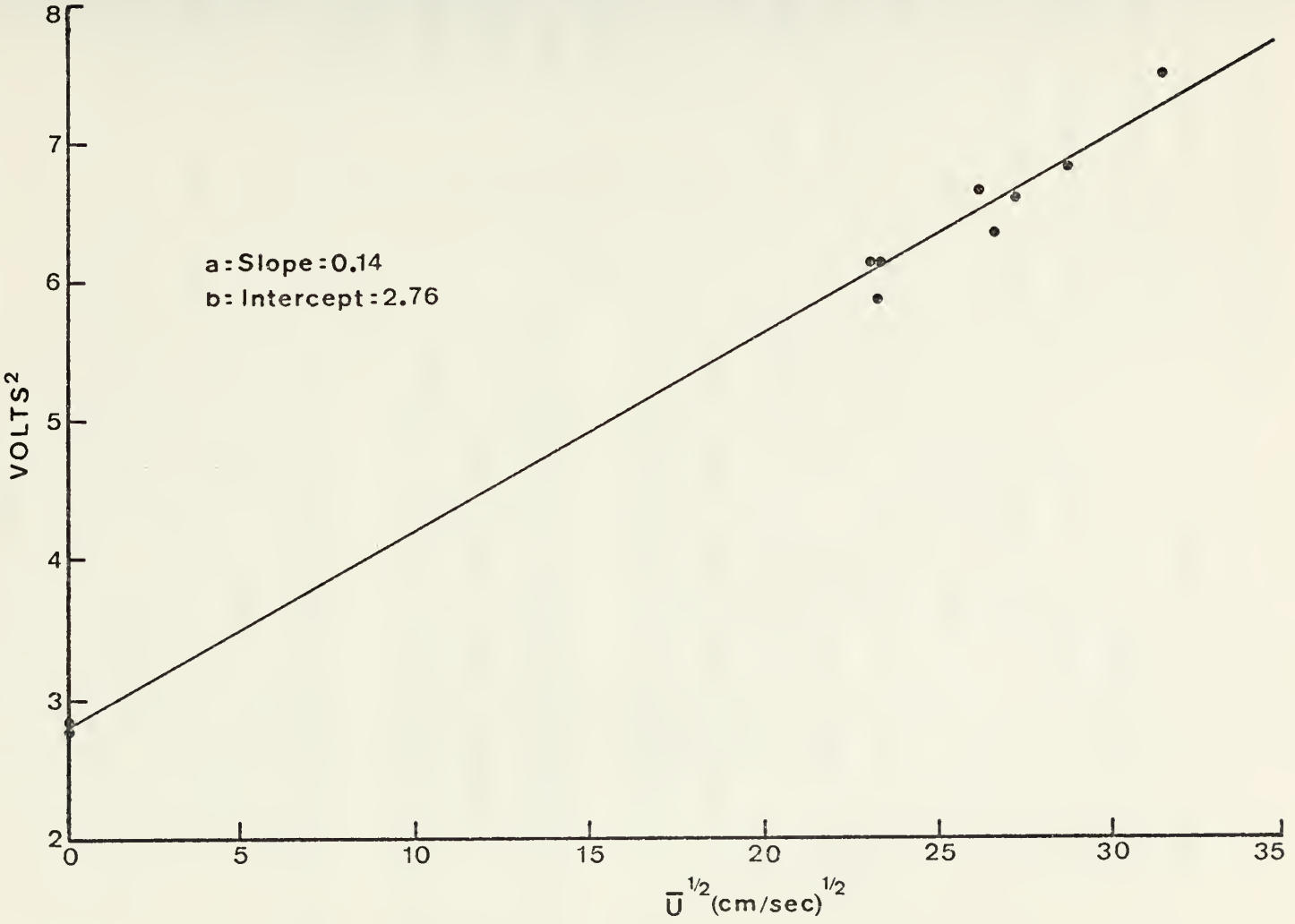

Figure 16. Hot wire in-situ calibration plot.

IV. RESULTS

A. FRICTION VELOCITY RESULTS

Friction velocity, U_*, was calculated in two ways. In the first method (method one) profiles of Ln (z) versus mean wind, $\overline{U}$, were plotted. Several examples of profiles are given in Figures 17, 18, and 19.

The best-fit profile for each time period was determined subjectively. When the sensor at a given level was known to be faulty or was highly suspect it was disregarded. When two very different possible profiles existed at any one time, levels 1 and 4 were used to determine the profile. Only 4 out of 41 periods were treated in such a manner. On only a few other occasions was a particular level considered erroneous. In a similar study by Smedely (1975) profiles were drawn using a least squares fit to the data.

After the profiles were drawn, 5 and 10 meter wind speeds were read from the profiles for each period and these values were used to solve Equation (7) for U_*. The results of these calculations for each period are shown in Table II as U_{*_p}.

Friction velocity was also calculated from fluctuation data (method two). First, Equation (23) was solved to obtain a value for the viscous molecular turbulent kinetic energy dissipation rate, ε, at each level. Then Equation (13) was solved to yield U_*. Ideally U_* at all levels would be equal for any given period since U_* was assumed to be constant in the surface layer. In fact, equipment failure or insensitivity, periods of nonneutral atmospheric conditions and the finite mathematics of computers combined to create less than ideal results.

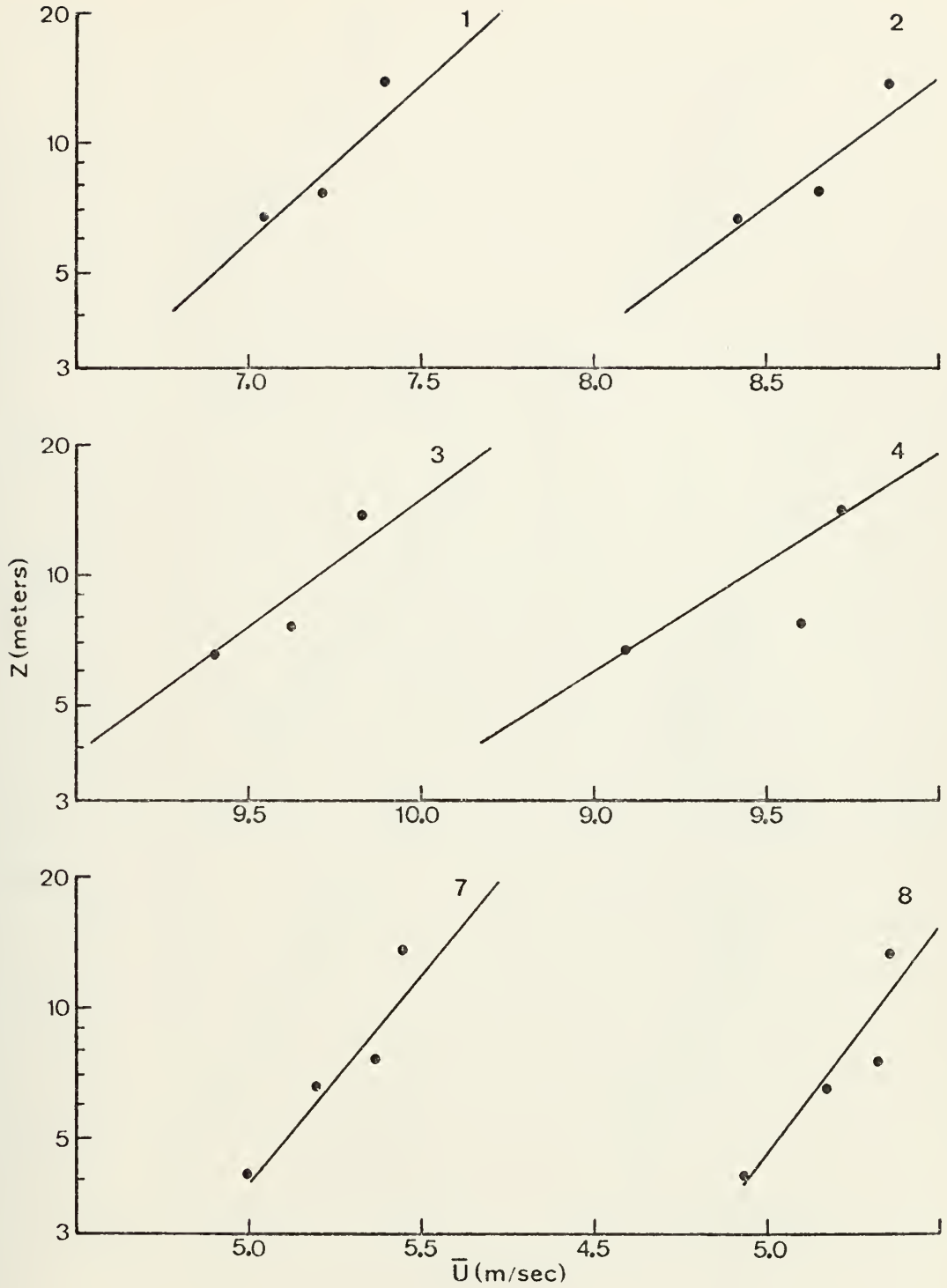

Figure 17. Profiles of mean wind, $\bar{U}$, versus Ln(z).

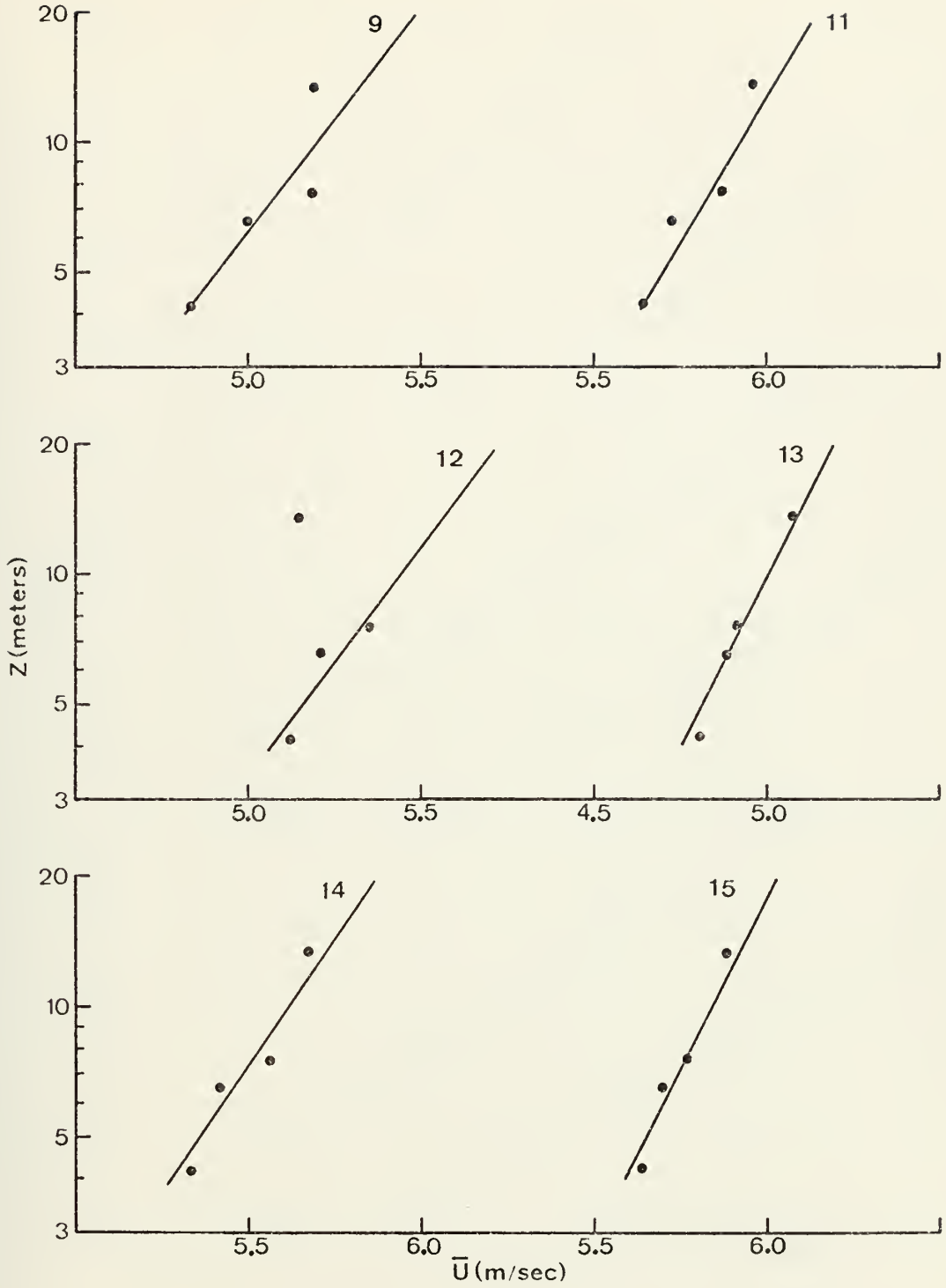

Figure 18. Profiles of mean wind, $\bar{U}$, versus Ln(z).

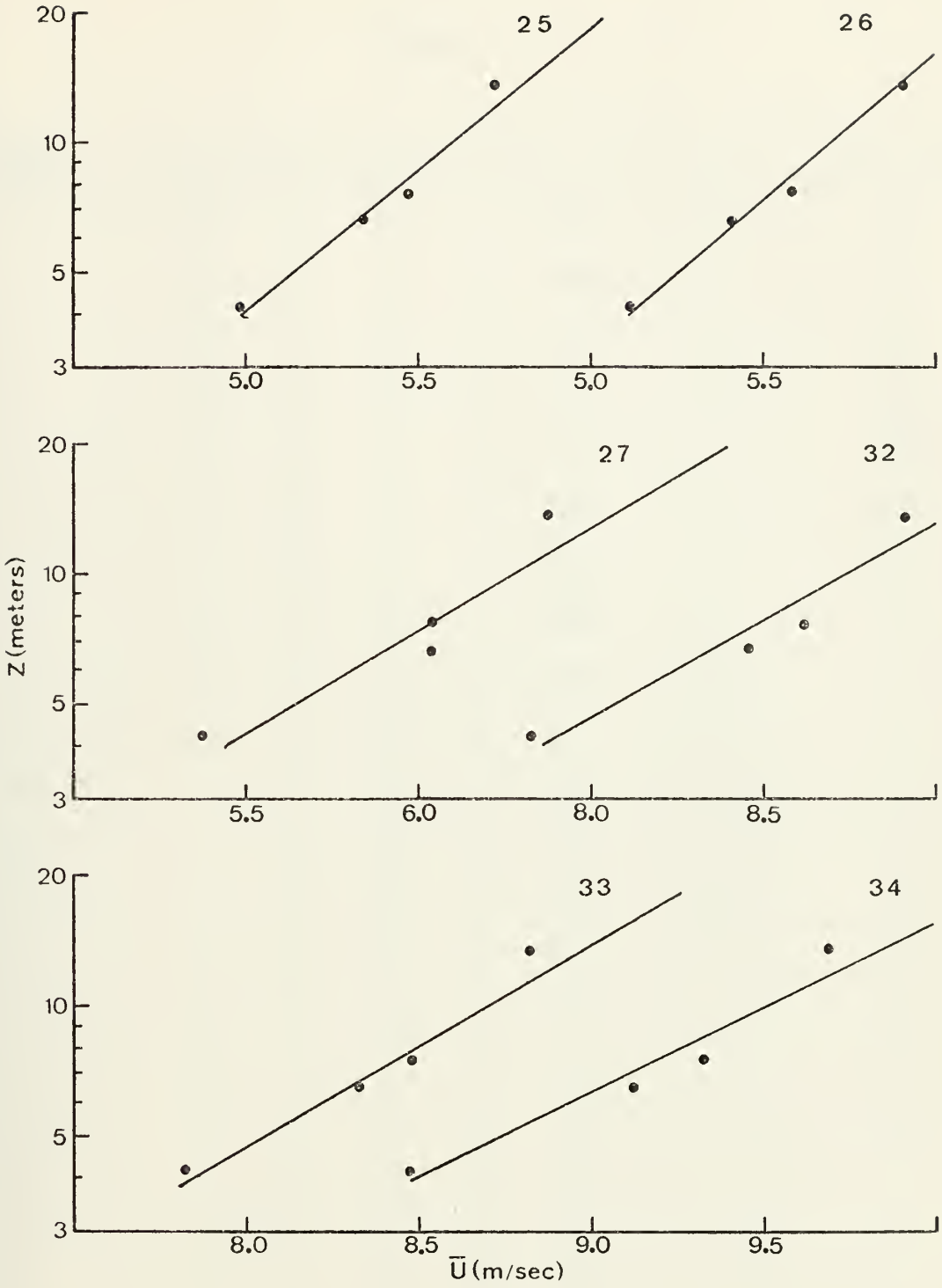

Figure 19. Profiles of mean wind, $\overline{U}$, versus Ln(z).

TABLE II

*PERIOD NUMBER	U_{*p}(m/sec)	$U_{*\varepsilon}$(m/sec)	$C_{10p} \times 10^3$	$C_{10\varepsilon} \times 10^3$	$\overline{U}_{10}$(m/sec)
1	.21	.28	0.82	1.50	7.32
2	.26	.33	0.88	1.40	8.75
3	.27	.44	0.78	2.10	9.69
4	.43	.42	2.00	2.00	9.45
5	.11	.20	0.53	1.70	4.82
6	.22	.33	1.40	3.20	5.81
7	.16	.14	0.90	0.67	5.40
8	.15	.16	0.81	0.90	5.33
9	.15	.15	0.85	0.85	5.20
10	.14	.20	0.88	1.80	4.71
11	.17	.25	0.80	1.70	6.00
12	.14	.20	0.68	1.40	5.43
13	.10	.25	0.40	2.50	5.02
14	.13	.18	0.54	1.00	5.61
15	.07	.20	0.15	1.20	5.78
16	.08	.17	0.22	1.00	5.38
17	.12	.24	0.30	1.20	6.87
18	.10	.26	0.38	2.60	5.13
19	.08	.19	0.31	1.80	4.52
20	.10	.13	1.40	2.60	2.53
21	.08	.13	1.10	2.90	2.41
22	.10	.17	0.54	1.60	4.30

TABLE II (continued

*PERIOD NUMBER	U_{*p} (m/sec)	$U_{*\varepsilon}$ (m/sec)	$C_{10p} \times 10^3$	$C_{10_\varepsilon} \times 10^3$	$\bar{U}_{10}$ (m/sec)
23	.03	.16	0.07	1.80	3.73
24	.31	.20	2.80	1.10	5.90
25	.25	.19	2.00	1.10	5.63
26	.23	.17	1.60	0.89	5.70
27	.32	.20	2.60	1.00	6.28
28	.27	.15	2.40	0.76	5.44
29	.19	.14	2.10	1.10	4.23
30	.15	.14	1.40	1.30	3.89
31	.15	.15	1.20	1.20	4.34
32	.34	.28	1.50	1.00	8.75
33	.33	.25	1.40	0.83	8.70
34	.39	.29	1.70	0.93	9.50
35	.42	.38	1.80	1.50	9.97
36	.64	.39	3.20	1.20	11.36
37	.55	.48	2.10	1.60	11.90
38	.26	.20	2.20	1.30	5.58
39	.38	.22	2.90	0.99	7.00
40	.31	.22	3.10	1.60	5.57
41	.27	.22	2.00	1.30	6.08

* Refer to Table I for dates and times.

Thus when all values of U_{*_ε} for any given period were within 20% of each other a linear average was taken to obtain a representative value for U_*. When values at any of the 4 levels differed by more than 20% adjacent periods were examined when possible in an attempt to determine a trend or isolate a bad level or levels. If no comparison was possible the two or three values that agreed most closely were averaged. The results of these calculations are listed in Table II as U_* .

Figure 20 is a plot of U_{*_p} versus U_{*_ε}. It shows little agreement between the mean-parameter approach and the fluctuation-parameter approach for calculating U_*. This lack of agreement might have arisen in part from the fact that mean data in this study was analyzed subjectively while the fluctuation data was analyzed electronically.

In connection with this lack of agreement, an analytical study of possible sensor motion at level 4 resulting from platform roll and pitch was conducted. The study showed that vertical motion of the platform probably had no significant effect on sensor position until roll or pitch or a combination of both exceeded 15°. However, under light wind conditions particularly, the lateral motion of the anemometers could result in erroneously high readings.

B. DRAG COEFFICIENT RESULTS

The friction velocity results were used to compute the momentum drag coefficient, C_{10}. Equation (19) was solved for C_{10} at the 10 meter level using first U_{*_p}, then U_{*_ε}. The results of these computations are contained in Table II. Figures 21 and 22 show plots of $\overline{U}_{10}$ versus C_{10p} and $C_{10\varepsilon}$ respectively. The curve from Cardone (1969) is plotted for comparison.

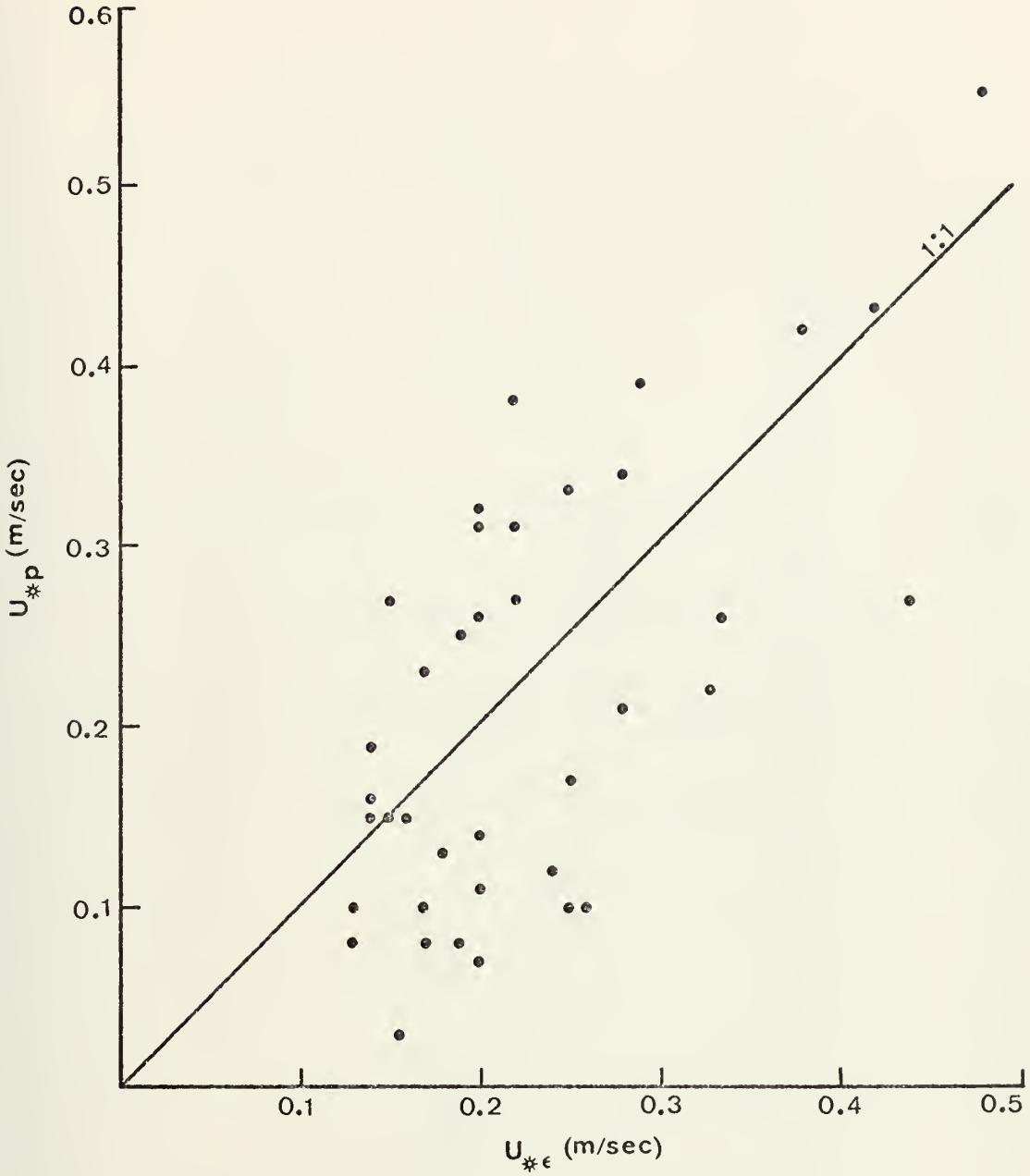

Figure 20. Comparison of friction velocity from Equation (13), $U_{*\epsilon}$, with friction velocity from Equation (7), U_{*p}.

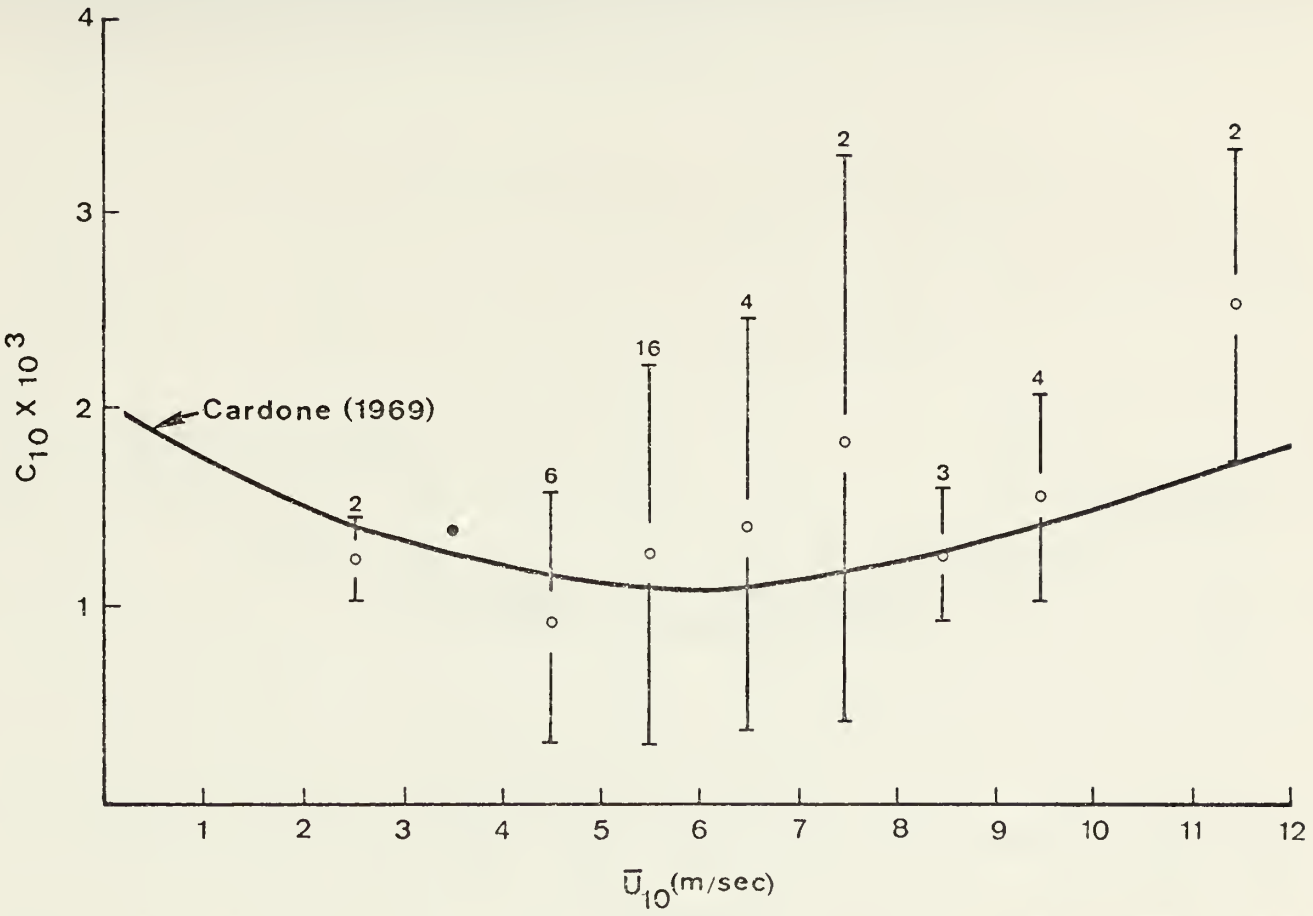

Figure 21. Plot of drag coefficient, C_{10p}, against mean wind speed, $\bar{U}_{10}$, at 10 meters. Average values of C_{10} correspond to 1 m/sec intervals.

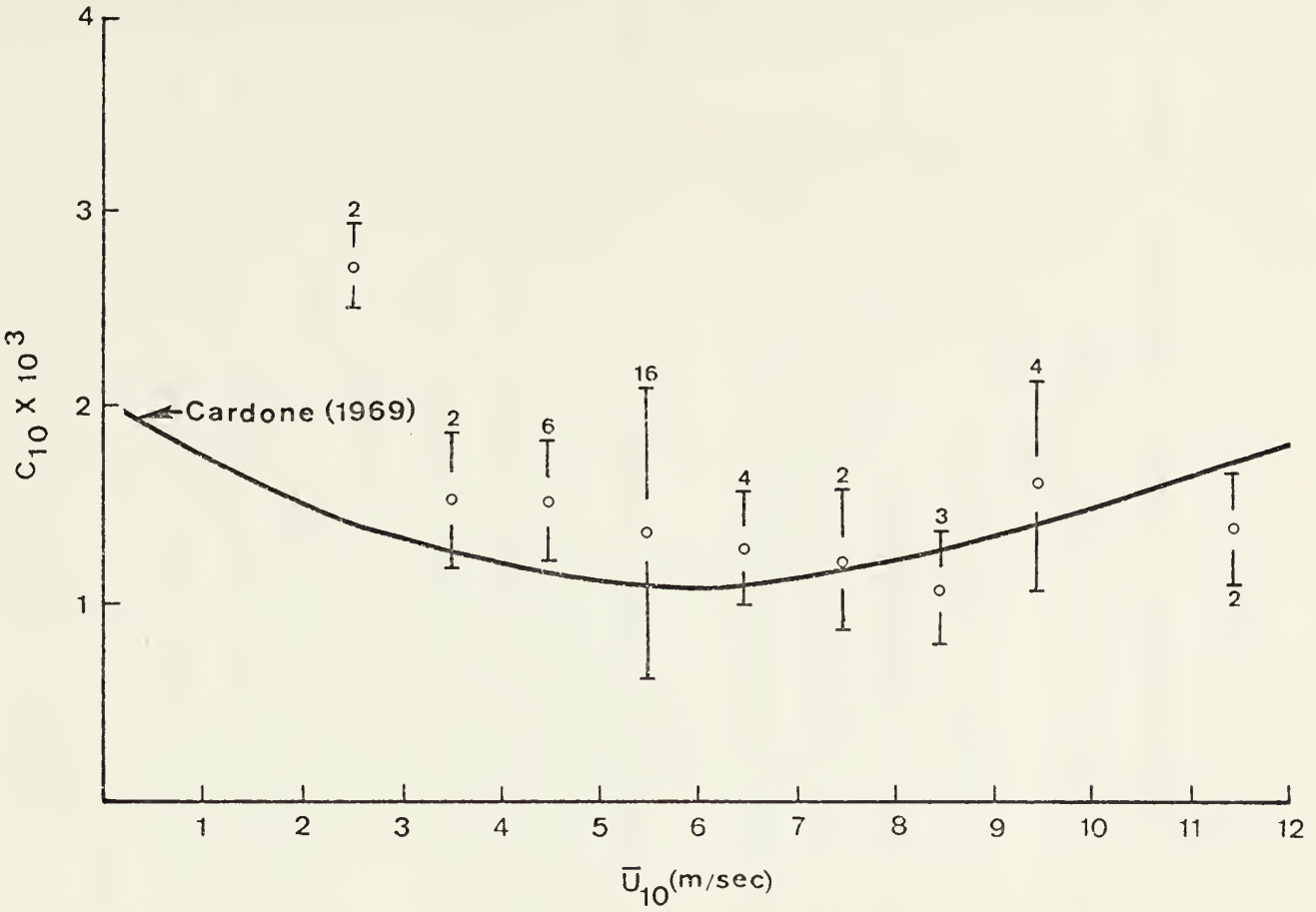

Figure 22. Plot of drag coefficient, $C_{10\varepsilon}$, against mean wind speed, $\bar{U}_{10}$, at 10 meters. Average values of C_{10} correspond to 1 m/sec intervals.

There appears to be credible agreement between Cardone (1969) and the $C_{10\varepsilon}$ results from this study. This lends credence to the U_{*_ε} results over the U_{*_p} results in this study.

C. HEAT FLUX ANALYSES

Atmospheric surface layer heat flux ($\overline{w'T'}$) was calculated using two different methods. Method one involved the use of fluctuation data to determine the heat flux. Method two employed the bulk aerodynamic approach as described by Friehe (1976).

The first method (method 1) required the calculation of the viscous molecular turbulent kinetc energy dissipation rate, ε, using Equation (23). Then using values for C_T^2 obtained from Highes (1976), Equation (16) was solved for ($\overline{w'T'_1}$). Table III lists the results of these calculations as ($\overline{w'T'_1}$).

Periods 30, 31, and 37 had values of 0 for ($\overline{w'T'_1}$) because $\partial\theta/\partial\theta$ was found to be essentially equal to 0. Here $\partial\theta/\partial z$ was calculated by Hughes (1976) from mean temperature profiles drawn for each period considered. Period 38 lacked temperature fluctuation data necessary for the calculation of C_T^2 used in the calculation of ε.

For all periods, ($\overline{w'T'}$) was calculated for each level where C_T^2 values were available. Next a representative value for ($\overline{w'T'_1}$) in the surface layer was obtained by a method similar to that used to obtain a mean value of U_* in section IV.A. of this study. In any given period values within 20% of each other were averaged. Adjacent periods were inspected for possible trends when necessary.

The heat flux calculated with method one was used to solve Equation (1) with $T_0 = \overline{T}_{10} + 273°C$. Then z/L was calculated at each level for every period where ($\overline{w'T'_1}$) was available and the results were plotted

TABLE III

*PERIOD NUMBER	$\overline{w'T_1'} \times 10^2$ (°C-m/sec)	$\overline{w'T_2'} \times 10^2$ (°C-m/sec)	$T_s - T_{10}$(°C)
1	-0.76	-2.17	-3.25
2	-0.48	-2.68	-3.36
3	-1.84	-3.06	-3.47
4	-2.33	-3.19	-3.71
5	-5.29	-0.56	-1.27
6	-8.77	-1.35	-2.56
7	1.10	a	a
8	0.62	a	a
9	0.45	a	a
10	-0.18	-0.18	-0.41
11	2.14	0.25	0.45
12	3.39	0.32	0.65
13	1.76	0.27	0.60
14	3.28	0.33	0.65
15	0.85	0.33	0.63
16	0.18	0.18	0.37
17	2.11	0.26	0.42
18	1.14	0.36	0.76
19	1.96	0.58	1.41
20	1.41	0.37	1.60
21	1.13	0.35	1.60
22	6.94	0.61	1.55

TABLE III (continued)

*PERIOD NUMBER	$\overline{w'T'_1} \times 10^2$ (°C-m/sec)	$\overline{w'T'_2} \times 10^2$ (°C-m/sec)	$T_s - T_{10}$(°C)
23	1.83	0.57	1.67
24	-1.40	0.36	-0.68
25	-3.22	-0.32	-0.62
26	-4.51	-0.29	-0.56
27	-7.83	-0.27	-0.48
28	-8.46	-0.06	-0.12
29	-26.60	0.02	-0.03
30	0	0.02	0.07
31	0	0.02	0.05
32	-21.90	0.53	0.67
33	-10.05	0.21	0.26
34	68.20	0.55	0.64
35	32.00	0.58	0.64
36	1.25	0.63	0.61
37	0	0.37	0.34
38	b	-0.46	-0.91
39	-2.21	-0.71	-0.11
40	-0.15	-0.34	-0.66
41	-4.55	-0.30	-0.55

* Refer to Table I for dates and times.

a $\overline{w'T'}_2$ not calculated due to lack of accurate surface temperature

b $\overline{w'T'}_1$ not calculated due to lack of temperature fluctuation data

against Ri values obtained from Hughes (1976). Figure 23 is a summary of these results. There seems to be little agreement with the curve from Businger et al. (1971).

Method two employed the bulk aerodynamic approach as described by Friehe (1976). Mean temperature profiles were used to determine $(\overline{T}_s - \overline{T}_{10})$. Table III lists values of $(\overline{T}_s - \overline{T}_{10})$ for all periods except 6, 7, and 8 when surface temperature was considered erroneous. Then Equation (17) was solved for $(\overline{w'T'_2})$ with selection of the appropriate constant, C_H, based on the value of $\overline{U}\Delta\overline{T}$. Results of these calculations are shown in Table III as $(\overline{w'T'_2})$.

Figure 24 shows a plot of $(\overline{w'T'}_1)$ versus $(\overline{w'T'}_2)$. The lack of agreement between $(\overline{w'T'}_1)$ and $(\overline{w'T'}_2)$ reiterates the general lack of agreement between the mean and fluctuation methods using the data available for this study.

Finally, the bulk method of calculating L was used to develop a second estimate of z/L. There Equation (18) was solved for 1/L and then z/L was developed for all 4 levels for all periods except 6, 7, and 8, when accurate temperature data was lacking. Figure 25 is a summary plot of z/L versus Ri where L was calculated with the bulk method. Comparison of results from this method with Businger et al. (1971) results yields no better agreement than the previous case although there appears to be a definite trend for the bulk method results.

Mean temperature profiles used to determine $\overline{T}_{10}$ for use in the bulk method were developed in the same way that mean wind profiles were developed as discussed in section IV.A. of this study. The mean temperature values from levels 1 through 4 for each time period were plotted against Ln(z). The best straight line fit to these points was drawn subjectively.

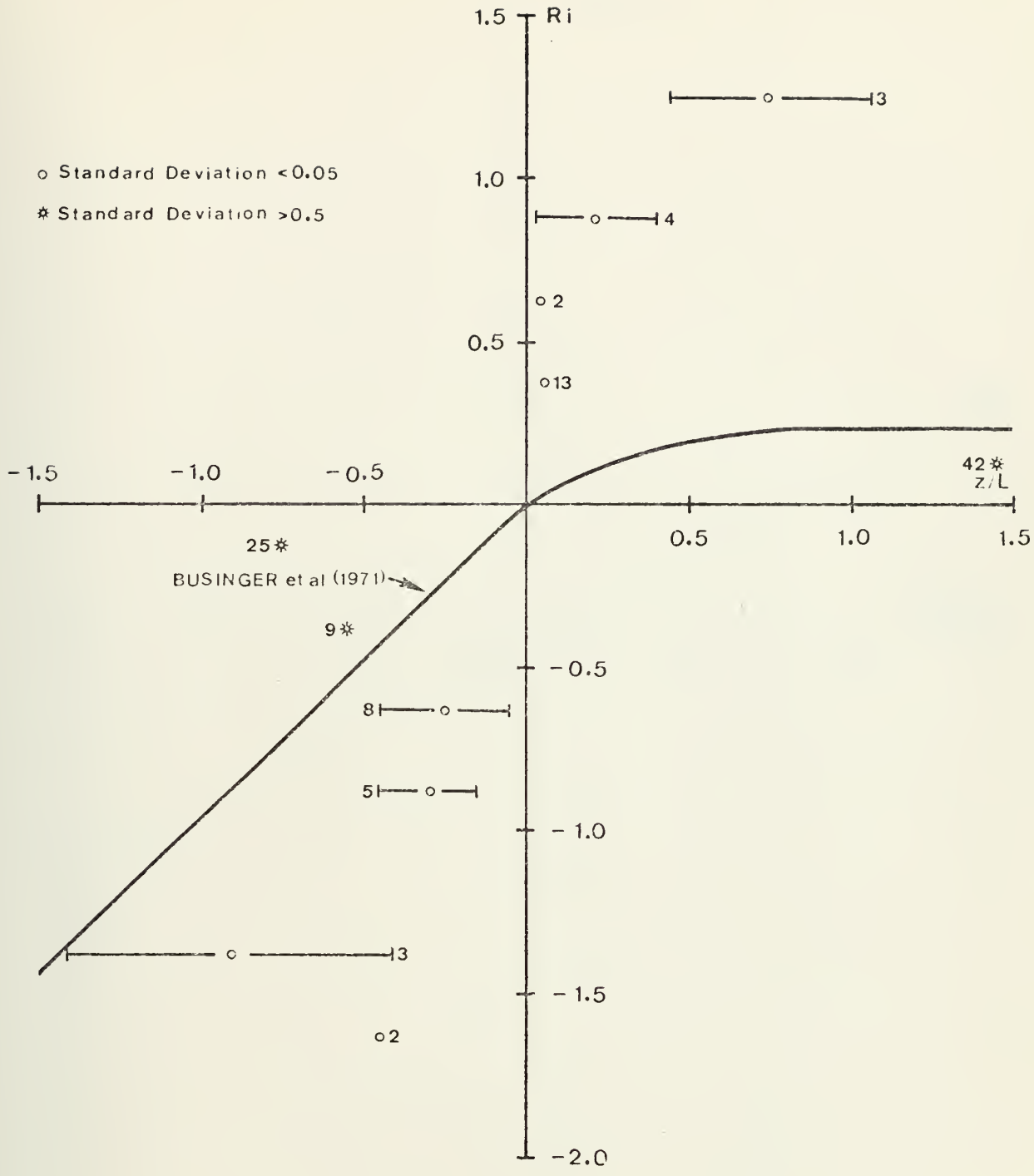

Figure 23. Comparison of z/L from Equation (1) with Ri. Average values of z/L correspond to 0.25 Ri intervals.

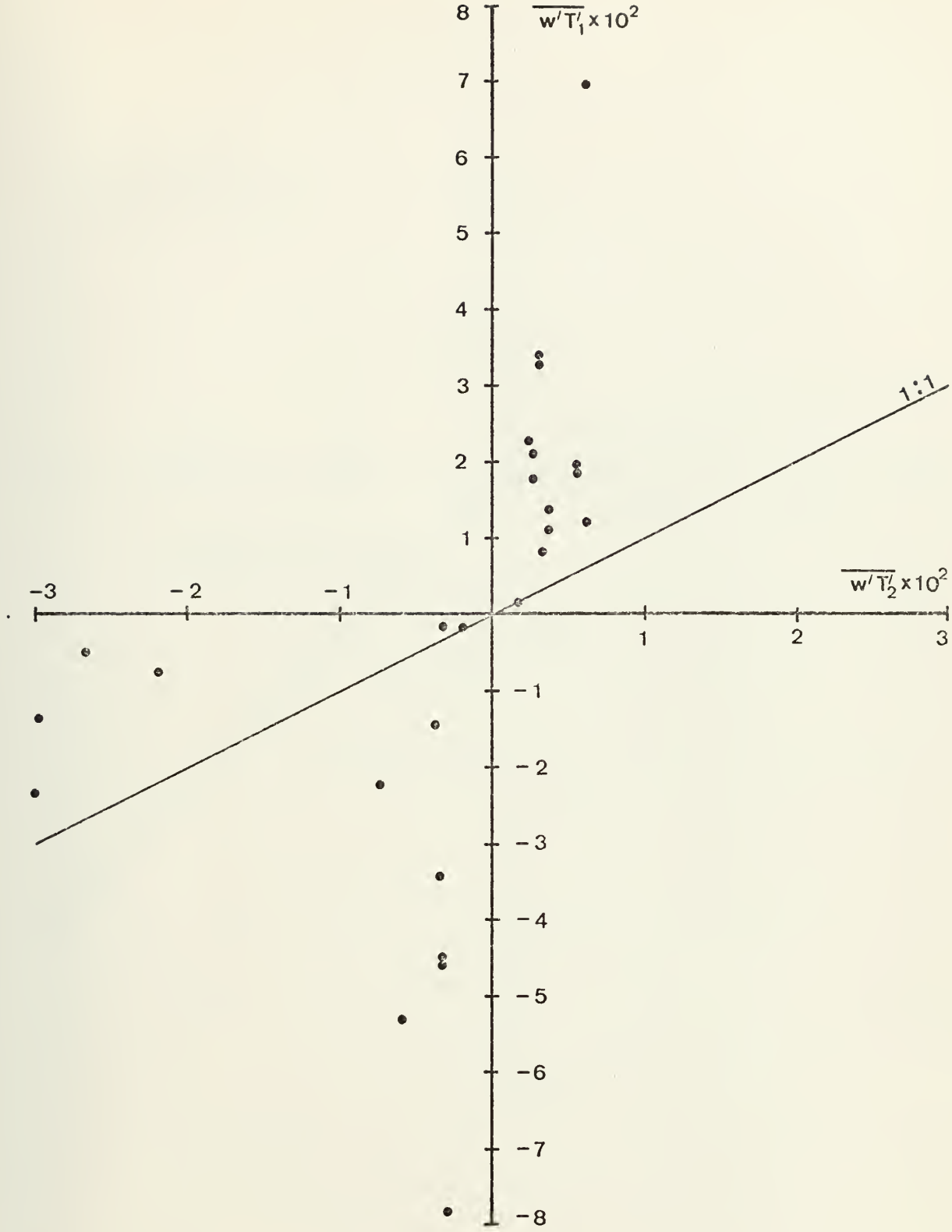

Figure 24. Comparison of sensible heat flux ($\overline{w'T_1'}$) from Equation (15) with sensible heat flux ($\overline{w'T_2'}$) from Equation (17).

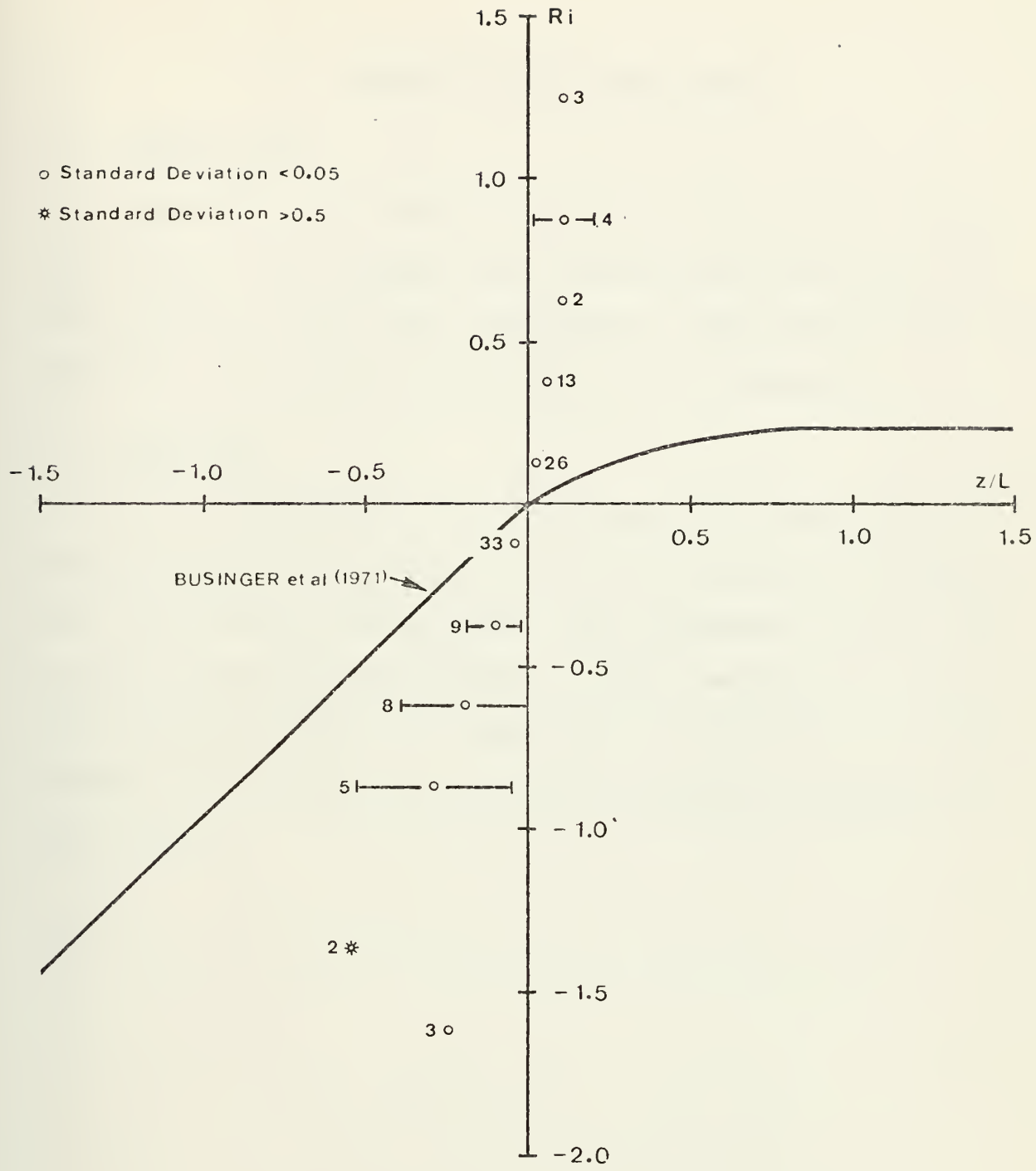

Figure 25. Comparison of z/L from Equation (18) with Ri. Average values of z/L correspond to 0.25 Ri intervals.

V. RECOMMENDATIONS AND CONCLUSIONS

A. RECOMMENDATIONS

Information on sea conditions would help in determining an average ship's motion. This information would be especially valuable under low wind conditions, because under such conditions sensor movement could cause significant sensing errors, particularly with the anemometers.

B. CONCLUSIONS

In conclusion, there is insufficient data at the present time to accurately evaluate the R/V Acania as a platform from which to study surface layer turbulence over the ocean. Many improvements have been made in the instrumentation and associated equipment used aboard R/V Acania since the data examined in this study were obtained. Future data should be more accurate and thus may yield better agreement in comparisons with other results.

LIST OF REFERENCES

1. Businger, J.A., J.C. Wyngaard, Y. Szumi and E.F. Bradley, 1975: "Flux-Profile Relationships in the Atmospheric Surface Layer", J. Atmos. Sci., 28, 184-189.

2. Cardone, V.J., 1969: "Specification of the Wind Distribution in the Marine Boundary Layer for Wave Forecasting", New York University, School of Engineering and Science, Scientific Report GSL-TR69-1, University Heights, New York, 131 pp.

3. Corrsin, S., 1951: "On the Spectrum of Isotropic Temperature Fluctuations in an Isotropic Turbulence", J. Appl. Phys., 22, 469-473.

4. Dyer, A.J. and B.B. Hicks, 1970: "Flux Gradient Relationships in the Constant Flux Layer", Q.J. Roy. Meteor. Soc., 96, 715-721.

5. Friehe, C.A., 1976: "Parameterizations of the Air-Sea Interface Fluxes of Sensible Heat and Moisture by Bulk Aerodynamic Formulae", Applied Optics, To be published.

6. Hughes, M., 1976: Investigation of Optically Relevant Turbulence Parameters, M.S. Thesis, Naval Postgraduate School, Monterey, California, 66 pp.

7. Lund, A.B., 1975: Spectral Estimates of Marine Turbulence Data, M.S. Thesis, Naval Postgraduate School, Monterey, California, 63 pp.

8. Monin, A.S., and A.M. Obukhov, 1954: "Basic Laws of Turbulent Mixing in the Ground Layer of the Atmosphere", Akademiia Nauk SSSR, Leningrad, Geofizicheskii Institut, Trudy No. 24(151), 163-187, English Translation by Miller, J., 1959.

9. Panofsky, H.A., A.K. Blackadar, and G.E. McVehil, 1960: "The Diabatic Wind Profile", Q.J. Roy. Meteor. Soc., 86, 390-398.

10. Smedley, G.W. III, 1975: Investigation of Vertical Profiles of Mean Temperature, Wind and Humidity. M.S. Thesis, Naval Postgraduate School, Monterey, California, 44 pp.

11. Taylor, G.I., 1938: "The Spectrum of Turbulence", Proc. Roy. Soc., A164, 476.

12. Webb, E.K., 1964: "Ratio of Spectrum and Structure Function Constants in the Inertial Sub-Range", Q.J. Roy. Meteor. Soc., 90, 344-346.

INITIAL DISTRIBUTION LIST

		No. Copies
1.	Defense Documentation Center Cameron Station Alexandria, Virginia 22314	2
2.	Library, Code 0210 Naval Postgraduate School Monterey, California 93940	2
3.	Naval Oceanographic Office Library (Code 3330) Washington, D.C. 20373	1
4.	Director, Naval Oceanography and Meteorology Building 200, Washington Navy Yard Washington, D.C. 20374	1
5.	Professor Kenneth L. Davidson, Code 51Ds Department of Meteorology Naval Postgraduate School Monterey, California 93940	9
6.	Professor Thomas M. Houlihan, Code 59Hm Department of Mechanical Engineering Naval Postgraduate School Monterey, California 93940	2
7.	Dr. B. Katz, Code 213 Naval Surface Weapons Center White Oak Silver Spring, Maryland 20910	1
8.	Mr. Steve Rinard Department of Meteorology Naval Postgraduate School Monterey, California 93940	1
9.	Professor Dale F. Leipper Chairman, Department of Oceanography Naval Postgraduate School Monterey, California 93940	1
10.	R/V Acania Department of Oceanography Naval Postgraduate School Monterey, California 93940	1

11. Lieutenant Allan B. Lund 1
Naval Weather Service Facility
Fleet Post Office
Seattle, Washington 98762

12. Captain A. Skolnick 1
PMS 405
Naval Sea Systems Command
Washington, D.C. 20632

13. Lieutenant M.M. Hughes 1
SMC Box 1313
Naval Postgraduate School
Monterey, California 93940

14. Lieutenant Commander H. E. Atkinson III 1
Commander Cruiser-Destroyer Group 1
Fleet Post Office
San Francisco, California 96601